Palaeogeography, Palaeoclimatology, Palaeoecology 597 (2022) 111014

Contents lists available at ScienceDirect

Palaeogeography, Palaeoclimatology, Palaeoecology

journal homepage: www.elsevier.com/locate/palaeo

Middle to Late Jurassic palaeoclimatic and palaeoceanographic trends in the Euro-Boreal region: Geochemical insights from East Greenland belemnites

Madeleine L. Vickers [a,b,*], Iben W. Hougård [a], Peter Alsen [c], Clemens V. Ullmann [d], Mads E. Jelby [a], Michael Bedington [e], Christoph Korte [a]

[a] Department of Geosciences and Natural Resource Management, University of Copenhagen, Øster Voldgade 10, DK-1350 Copenhagen K, Denmark
[b] Centre for Earth Evolution and Dynamics (CEED), University of Oslo, P.O. Box 1028 Blindern, N-0315 Oslo, Norway
[c] Geological Survey of Denmark and Greenland, Øster Voldgade 10, DK-1350 Copenhagen K, Denmark
[d] Camborne School of Mines, University of Exeter, Penryn, Cornwall TR10 9FE, UK
[e] Plymouth Marine Laboratory (PML), Prospect Place, The Hoe, Plymouth PL1 3DH, United Kingdom

ARTICLE INFO

Editor: Dr. A Dickson

Keywords:
Belemnites
Carbon isotopes
Oxygen isotopes
Viking Corridor
Tethys
Boreal
VOICE

ABSTRACT

During the Middle and Late Jurassic, Europe and the Boreal regions formed a network of semi-restricted, relatively shallow marine basins. Consequently, stable oxygen ($\delta^{18}O$) and carbon ($\delta^{13}C$) isotope records from belemnites were strongly influenced by changes in palaeoceanography and climate. New data from eastern Greenland, which formed the western margin of the critical Viking Corridor (the narrow seaway that linked the Tethys to the Boreal realm), and compiled data from the Subboreal Province and Tethys Realms are examined together. In both territories, increases in $\delta^{18}O_{bel}$ across the Lower and Middle Jurassic boundary indicate that cooling occurred, although this appears to be temporally offset and of variable magnitude across the western Subboreal Province and Tethys Realm. This suggests that changes in ocean current patterns played a major role in governing the $\delta^{18}O_{bel}$ signal. The Middle to Upper Jurassic transition is characterised by relatively heavy $\delta^{18}O_{bel}$ values in the Subboreal Province, but is less pronounced in the northwest Tethys, suggesting that this trend may have been caused by a strengthening of a southward current bringing colder Boreal waters southwards. The uppermost Jurassic shows increases in both $\delta^{18}O_{bel}$ and $\delta^{13}C_{bel}$, consistent with the observed VOICE event as recorded in Boreal terrestrial organic matter $\delta^{13}C$, and supporting this evidence that the Boreal realm become isolated from the lower latitudes across the Jurassic – Cretaceous boundary.

1. Introduction

The break-up of the supercontinent Pangaea during the Middle and Late Jurassic led to dramatic changes in oceanography, which in turn governed equator-to-pole heat transport, extent of species area and degree of provincialism, and regional to global climatic conditions. The narrow seaway of the Viking Corridor formed during this period of continental break-up, and connected the Boreal Realm with the Tethys Realm (Fig. 1; Torsvik et al., 2002). During the Jurassic, the Viking Corridor was variably open or closed (e.g. Doré, 1991; Torsvik et al., 2002; Callomon, 2003; Page, 2008), which markedly affected marine palaeobiogeographic distribution patterns and potentially regional to global climatic and environmental trends (e.g. Page, 2008; Nunn et al., 2009; Price and Rogov, 2009; Nunn and Price, 2010; Korte et al., 2015; Georgiev et al., 2017; Wierzbowski et al., 2018; Rogov et al., 2020; Vickers et al., 2020). These changes in climate and circulation are documented in the stable oxygen ($\delta^{18}O$) and carbon ($\delta^{13}C$) isotopic signatures of calcifying organisms, and in the carbon stable isotopes of organic matter. Among the marine calcifiers, belemnites, bivalves and brachiopods are frequently used in Jurassic studies due to their ubiquitous spread across high to low latitudes, and their high preservation potential (Veizer et al., 1999; Jenkyns et al., 2002; Dutton et al., 2007; Dera et al., 2011; Alberti et al., 2012; Wierzbowski et al., 2013; Korte et al., 2015). Yet, it rapidly became apparent that belemnites recorded different isotopic values than co-occurring non-cephalopod molluscs (e.g. Voigt et al., 2003; Dera et al., 2011). In part, this is likely due to their

* Corresponding author at: Centre for Earth Evolution and Dynamics (CEED), University of Oslo, P.O. Box 1028 Blindern, N-0315 Oslo, Norway.
E-mail address: m.l.vickers@geo.uio.no (M.L. Vickers).

https://doi.org/10.1016/j.palaeo.2022.111014
Received 14 November 2021; Received in revised form 12 April 2022; Accepted 20 April 2022
Available online 25 April 2022

different habitats, as belemnites were free-swimming and different genera are believed to have inhabited different water depths, with many being pelagic (e.g. Klug et al., 2016; Hoffmann and Stevens, 2019; Vickers et al., 2019, 2021), whereas bivalves and brachiopods are benthic organisms. Thus, sedimentologically co-occurring belemnites and benthic calcifiers were precipitating their shells from different water depths, with bottom waters expected to be colder and have potentially different $\delta^{18}O_{sw}$ to photic-zone waters. However, contradictorily, belemnites consistently show the same or "cooler" $\delta^{18}O$ than co-occurring benthic organisms (e.g. Voigt et al., 2003; Dera et al., 2011). Recent work has shown that belemnites fractionate ^{18}O differently to other molluscs, and therefore direct comparison between belemnites and other molluscan isotope records cannot be made (Bajnai et al., 2020; Vickers et al., 2021), although trends in the records may be compared (Korte and Hesselbo, 2011). Examination of the belemnite stable isotope record can reveal information about temporal and spatial palaeo-oceanographic and climate trends in the upper part of the water column. Yet, caution must be used when interpreting $\delta^{18}O$ trends as both changes in salinity and temperature affect the $\delta^{18}O$ of calcite, which may dampen or magnify the signal recorded (e.g. Wierzbowski et al., 2018; Vickers et al., 2020). As Europe was essentially a series of restricted basins during the Jurassic (Fig. 1), the basins were likely to have seen strong changes in salinity, linked to changes in paleocurrent directions and climate-related changes in the hydrological cycle, making it often very difficult to untangle climatic and palaeoceanographic signals.

This study investigates the magnitude, duration and spatial extent of stable isotopic perturbations in the northern hemisphere during the Middle and Late Jurassic (Fig. 1), through examining belemnite stable isotope trends from the western margin of the crucial Viking Corridor, and comparing them to compiled data from the Boreal Realm, Subboreal Province and Tethys Realm. We discuss the possible relative influence of changes in palaeoceanography and climate to the stable isotope records of the broader Euro-Boreal region.

1.1. Geological setting

Jurassic sedimentary rocks along the western margin of the Viking Corridor are exposed in the coastal ice-free areas of East and North-East Greenland along a ca. 700 km long stretch from Jameson Land in the south to Store Koldewey in the north (Fig. 1B).

A relatively complete upper Triassic–lowermost Cretaceous succession is preserved in the Jameson Land Basin, whereas the areas north of Jameson Land only include Middle and Upper Jurassic sedimentary rocks. The Lower Jurassic succession of Jameson Land was deposited in a gently subsiding basin during thermal contraction, and comprises the organic-rich Ostreaelv and Sortehat Formations. Subsidence became differentiated and asymmetric with the initiation of a major rift phase in the Bajocian (Middle Jurassic) with greater subsidence to the west (Surlyk et al., 2021). The configuration of the southern Jameson Land Basin was largely a gently tilted platform, whereas the north was characterised by half-graben rift basin geometry (Fig. 1B; Surlyk, 2003; Surlyk et al., 2021). This is particularly evident in the Wollaston Foreland Basin (Surlyk, 1978). The sedimentary strata reflect northwards younging on progressively older rocks with Triassic strata in the south and crystalline peneplaned basement in the north. This onlap toward the north may reflect late Early Jurassic domal uplift in northern North-East Greenland, with subsequent erosion of the dome followed by the Middle Jurassic rifting and transgression (Surlyk, 1977, 1978; Surlyk et al., 2021).

The Middle Jurassic succession of the Jameson Land and Wollaston Foreland basins is dominated by shallow-marine sandstone (the widespread Pelion Formation) deposited in large embayments bordered to the east by peninsulas, which were controlled by the uplifted shoulders of inherited fault blocks tilted to the west (Surlyk, 1977).

Sea level rose during the Middle and Late Jurassic, and the succession accordingly forms an overall backstepping stacking pattern progressively fining upwards into offshore marine organic-rich mudstone

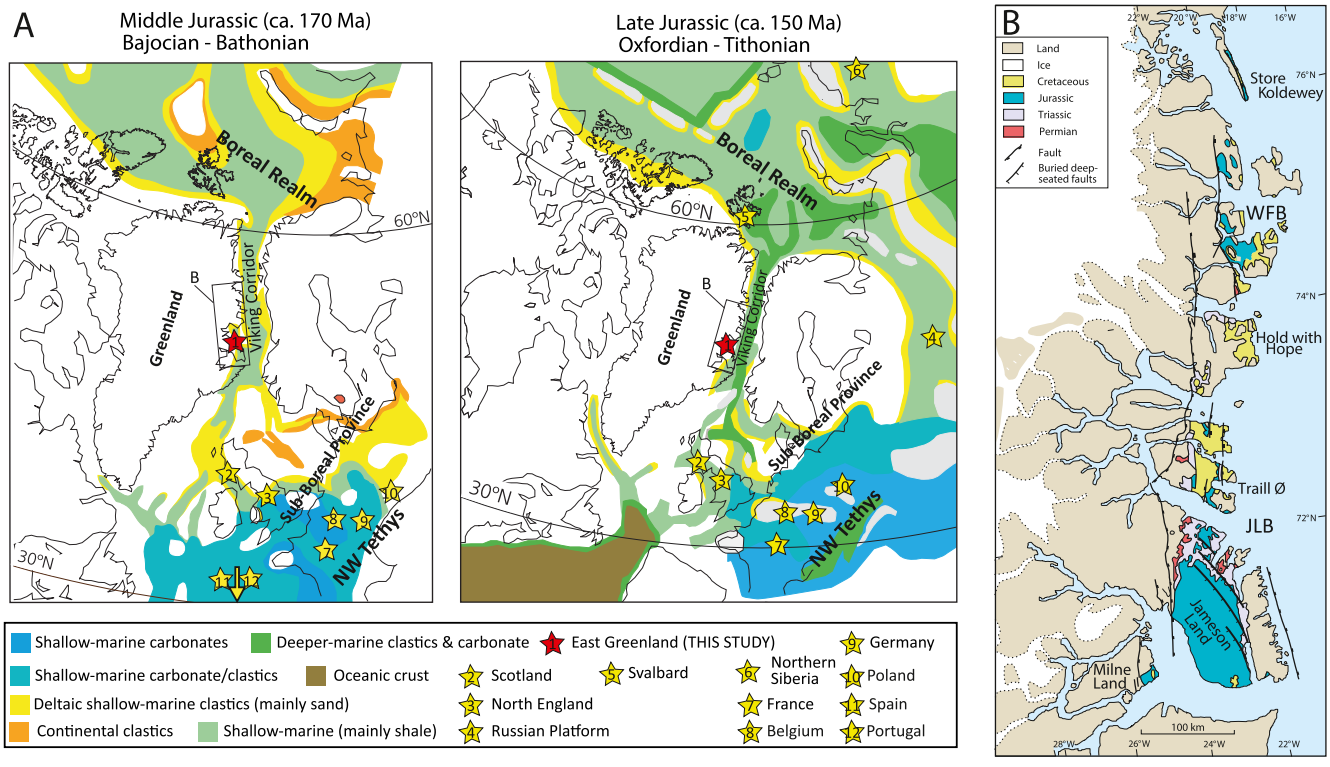

Fig. 1. Maps of the Viking Corridor palaeogeography and section distribution in the studied East Greenland basins. **(A)** Middle and Late Jurassic palaeogeography of the Euro-Boreal region (modified from Torsvik et al., 2002). The map for the Middle Jurassic indicates that shallow waters could potentially have constituted a barrier between the Arctic and Tethys Oceans. By the Late Jurassic, the seaway had reopened due to sea-level rise. **(B)** Geological map of East Greenland showing outcrops and distribution of the studied gross sedimentary basins (modified from Surlyk, 2003). JLB, Jameson Land Basin; WFB, Wollaston Foreland Basin.

reflecting deep and relatively tranquil deposition in the Kimmeridgian (Late Jurassic) (Surlyk, 2003). This came to an abrupt end in the latest Jurassic during middle–late Volgian maximum rifting that resulted in a 2 to 3 km thick, marine succession of coarse-grained gravity-flow deposits in the deepest parts of the half-grabens along the western major bounding fault (Surlyk, 1978; Surlyk et al., 2021).

2. Materials and methods

2.1. Materials

Belemnite samples were sourced from the Geological Survey of Denmark and Greenland (GEUS) sample archive, originally from the collections of M. Enkilde and P. Alsen, and are available to be loaned on request. The samples were collected during several fieldwork campaigns in East and North-East Greenland between 1990 and 2017, by a number of colleagues from the Geological Institute (now Department of Geosciences and Natural Resources Management), University of Copenhagen and GEUS. Much of the material from Jameson Land was compiled by M. Engkilde.

Due to the spread of the samples across five sub-regions of East Greenland and the difficulty in correlating outcrop sections, the samples were collected with stratigraphic reference to the ammonite faunal horizon, rather than with reference to a sedimentary log. In total, 79 low-Mg calcite belemnites were selected from five East Greenlandic sub-regions spanning palaeolatitudes of 50–55°N: Jameson Land, Milne Land, Traill Ø, Hold with Hope and Store Koldewey (Fig. 1B). The belemnites are not determined taxonomically but Jurassic belemnites from East Greenland typically belong to the Subboreal genera *Cylindroteuthis* and *Pachyteuthis* (Spath, 1932, 1935, 1936; Doyle, 1987), two genera which are believed to have inhabited the same water depths (Vickers et al., 2020).

The stratigraphic placement of the specimens is based on a compilation of Greenlandic ammonite biostratigraphy using the Lower Jurassic zonation of Koppelhus and Hansen (2003), the Middle Jurassic zonations of Callomon (1993, 2003) and Callomon et al. (2015), and the Upper Jurassic zonation of Surlyk (1978, 1991), Sykes and Callomon (1979), Callomon and Birkelund (1980), Birkelund et al. (1984), and Birkelund and Callomon (1985). Ammonites are limited in some sections in East Greenland, and where ammonites are not found, palynostratigraphy is used for age assessment instead (e.g. Piasecki and Stemmerik, 2004; Piasecki et al., 2004a, 2004b; Alsen and Piasecki, 2018). The palynostratigraphic events and ranges have been meticulously analysed within the ammonite stratigraphy, often with palynomorphs derived directly from ammonite samples, providing the closest possible correlation between ammonites and palynomorphs (Milner and Piasecki, 1996; Piasecki, 1996). Regional stratigraphic ties are based on correlation with the Russian Platform and with the Subboreal Province (Rogov, 2010; Hesselbo et al., 2020).

2.2. Sample screening

Surface examination of selected belemnite rostra were undertaken by secondary electron Scanning Electron Microscopy (SE SEM). Sub-millimetric solid pieces from the sampled rostral area were placed on SEM stubs. The stubs were gold-coated using a Polaron Equipment Limited SEM coating Unit E5000 to avoid electronic build-up during analysis. Examination of the crystal morphology was undertaken using backscattered electrons on an FEI Quanta Inspect 250 Scanning Electron Microscope under high vacuum of 1.8–2.2 μtorr and an electron beam with 95–97 μA current at 20 kV at the Geological Museum, Natural History Museum of Denmark, University of Copenhagen.

All samples were screened for diagenetic alteration using inductively coupled plasma-optical emission spectrometry (ICP-OES) analysis. For ICP-OES analysis, aliquots of 300–700 μg were weighed into plastic tubes. Samples were diluted with 2% nitric acid to a nominal Ca concentration of 25 μg/g and analysed for element/Ca ratios against a set of matrix-matching calibration solutions using an Agilent 5110 VDV ICP-OES at Camborne School of Mines, University of Exeter. Measurements were repeatedly controlled against certified reference materials and synthetic quality control solutions (see Ullmann et al., 2020 for full analytical detail).

2.3. Carbon-isotope and oxygen-isotope analyses

A total of 234 stable carbon-isotope and oxygen-isotope analyses were performed on the 79 belemnite rostra, whereby two to three sub-samples were collected per specimen. Additionally, one sub-sample of macroscopically visible diagenetically altered material was taken from the porous apical line of the rostra. This region of the rostra is believed to be representative of the diagenetic signal, because it typically contains a high percentage of infilled diagenetic sparry and/or recrystallised calcite (Ullmann et al., 2015). The dorsal side of belemnite rostra was preferentially taken for sampling and prepared following preparation techniques documented by previous authors in detail (Ullmann et al., 2013a). Analytical procedures by Spötl and Vennemann (2003) were adopted and performed using an IsoPrime Triple Collector Isotope Ratio Mass Spectrometer with continuous flow setup at the stable-isotope laboratory of the Department of Geosciences and Natural Resource Management, University of Copenhagen.

Belemnite rostra were drilled using a handheld drill with a diamond-sintered drill bit of approximately 1 mm diameter, and extracted sample material equivalent to 0.6 mg carbonate was placed into glass Labco vials and sealed with plastic lids. Vials were flushed with helium to remove atmospheric gasses and subsequently reacted with nominally anhydrous phosphoric acid at 70 °C for 90 min. The measured $^{13}C/^{12}C$ and $^{18}O/^{16}O$ ratios were normalised against a CO_2 reference gas. The reproducibility of the analyses was 0.04‰ for $\delta^{13}C$ (1 σ, n 84) and 0.06‰ for $\delta^{18}O$ (1 σ, $n = 84$) based on 15 standards to 45 samples in each batch of analyses. Isotope ratios were corrected with the in-house reference material LEO ($\delta^{13}C = +1.96‰$; $\delta^{18}O = -1.93‰$; see Ullmann et al., 2013a), which is calibrated to the international reference materials NBS-18 and NBS-19, ensuring accurate determination of isotope ratios.

2.4. Statistical treatment of the data

A generalised additive model (GAM) was fitted to the data to capture trends in the data through time. Only samples that passed the screening for diagenetic alteration were included in the estimation of stable isotope trends and the fit was undertaken against time, derived by binning the data into discrete biozones. The same method was used on a compilation of published data to compare trends across the Tethys and Boreal realms. The correlations between the Boreal, Subboreal, and Tethyan biozones are as given in Hesselbo et al. (2020).

A GAM was used in preference to other approaches, such as LOESS curve fitting, as it is more suitable for data with categorised predictor variables (in this case the age - the samples were binned into discrete biozones). The pyGAM package (Servén and Brummitt, 2018) was used to construct the GAM using an identity link function and normal distribution, with a single spline term and intercept. The number of splines (nspline parameter) was chosen apriori to reflect the variation in the data across the timescale studied using, for the stable isotope data, nspline = 25, with the exception of the southwest Tethys which represents a considerably shorter time period (nspline = 10). For the Sr/Ca data, npsline = 10 was chosen to show the lower resolution of variation observed in the record. The curve fit was then optimised using the PyGAM gridsearch function to find the optimal value for the Lambda parameter. This parameter is a penalty on the second derivative which ensures the smoothness of the curve. The confidence interval for the model was estimated using the confidence_interval method in pyGAM; this confidence interval is for the fit of the model given the data and

therefore primarily reflects the density of the data. Additionally, this method assumes that the smoothing parameters are fixed, whereas we have optimised the Lambda parameter based on the data which will tend to lead to an underestimation of the *p* value.

3. Results

3.1. Element concentrations and optical investigations

Ultra-structure examination under SE SEM shows, for most rostrum sub-samples, preservation of the obelisk-like morphology of the rostrum crystal, with rare occurrences of slight dissolution or recrystallisation (Fig. 2).

Strontium and manganese concentrations in belemnite rostrum can be used as proxies for diagenesis (e.g. Ullmann and Korte, 2015). The Sr/Ca ratios of the dataset range between 0.21 and 2.54 mmol/mol. A clear diagenesis trend occurs in the Sr/Ca ratios in altered apical-line samples, with progressively lower Sr/Ca ratios relative to more negative $\delta^{18}O$ values (Fig. 3A), although the variations are not large and in some cases Sr/Ca ratios may even be higher than ratios from rostrum samples (Fig. 3A).In the unaltered samples, highest Sr/Ca ratios occur in the Toarcian and decrease in the Middle Jurassic before increasing again in the Late Jurassic (Fig. 4).

In general, Mn/Ca ratios are significantly lower in rostrum samples compared to the apical-line samples. Mn/Ca ratios range between 8.27 and 0.0 mmol/mol, with the highest Mn/Ca ratios in the apical line sub-samples relative to adjacent sub-samples of the rostrum (Fig. 3B). The highest Mn/Ca ratios (0.03–0.31) in rostrum occur in belemnites from the organic-rich Aalenian–Bajocian Sortehat Formation.

High Mg/Ca ratios only occur in altered sub-samples. Correlation between $\delta^{18}O$ and $\delta^{13}C$ ratios show that lower $\delta^{13}C$ ratios coincide with negative $\delta^{18}O$ ratios in altered apical line subsamples (Fig. 3C).

3.2. Carbon-isotope and oxygen-isotope trends

The Greenland Jurassic belemnite $\delta^{18}O$ values (averaged per sample after screening for alteration) range from −4.03 to 1.50‰, with a mean of −0.54‰ (Fig. 4). The belemnites show a mean standard deviation of 0.41‰ between subsamples of the well-preserved specimens. The GAM shows lowest average $\delta^{18}O_{bel}$ in the Toarcian (although data are sparse), increasing to the Bajocian and remaining higher (c. -1) into the Oxfordian (Fig. 4). The data are fairly scattered in this interval, with most negative values occurring in the Bajocian and Bathonian and most positive values found in the upper Callovian. The GAM for the Upper Jurassic $\delta^{18}O_{bel}$ is almost invariable, with an average remaining constant around c. -1 (Fig. 4). Though the data is sparse in this interval, the

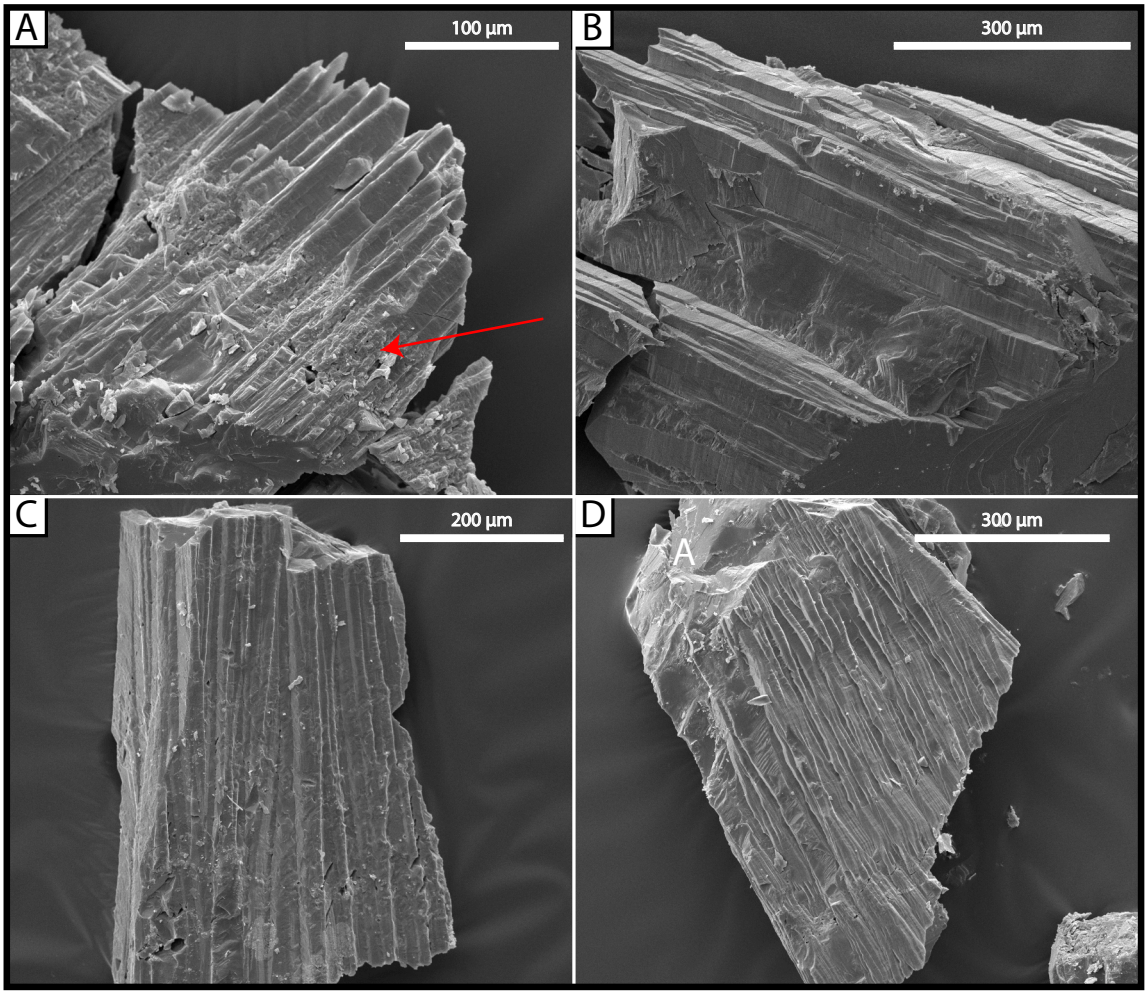

Fig. 2. Secondary electron (SE) scanning electron microscopy (SEM) images of belemnite rostra. **(A)** Well-preserved belemnite from the *C. pompeckji* Zone, Traill Ø, showing single crystal with obelisk-like morphology and the more porous growth band (red arrow). **(B)** Well-preserved belemnite from the *A. rosenkrantzi* Zone, Milne Land, showing single crystal with obelisk-like morphology. **(C)** Slightly dissolved crystals in a rostrum from the *K. jason* Zone, Hold with Hope. **(D)** Partially recrystallised rostrum from the *C. pompeckji* Zone, Traill Ø. (For interpretation of the references to colour in this figure legend, the reader is referred to the web version of this article.)

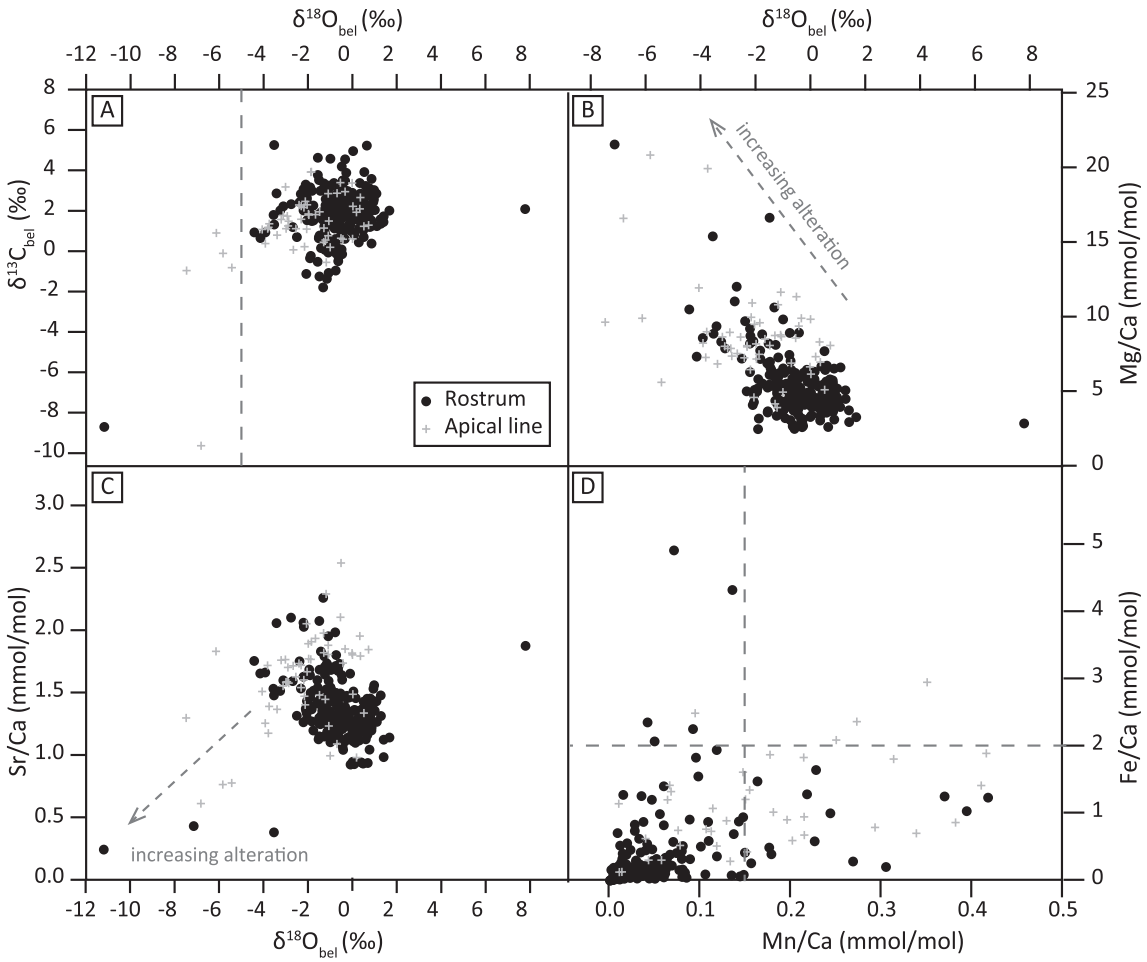

Fig. 3. Common proxies for diagenesis from altered apical line and rostrum samples, to evaluate the preservation degree of the belemnites. **(A)** Belemnite $\delta^{18}O$ plotted against $\delta^{13}C_{bel}$. Dashed line marks the cut-off $\delta^{18}O_{bel}$ value used to screen the published $\delta^{18}O_{bel}$ data. **(B)** Belemnite $\delta^{18}O$ plotted against belemnite Mg/Ca ratios. The apical line sub-samples show increasing Mg/Ca with decreasing $\delta^{18}O_{bel}$, but also greater spread in the values with decreasing $\delta^{18}O_{bel}$. Dashed arrow marks the interpreted diagenetic trend direction. **(C)** Belemnite $\delta^{18}O$ plotted against Sr/Ca. In the apical line subsamples there, more negative $\delta^{18}O_{bel}$ correspond to lower Sr/Ca ratios. **(D)** Belemnite Mn/Ca plotted against Fe/Ca ratios. Both apical line and non-apical rostral subsamples display the classic trend of roughly co-varying variables increasing scatter with higher ratios (e.g. Nunn and Price, 2010). Cut-off limits for screening the rostral samples are indicated by dashed lines.

scatter is lower throughout the interval than observed in the Middle Jurassic (Fig. 4).

The Greenland Jurassic belemnite $\delta^{13}C$ values, averaged for individual specimens, range from −0.71 to 4.55‰, with mean of 1.88‰ (Fig. 4). Individual belemnite specimens show a mean standard deviation of 0.44‰ between subsamples of the well-preserved regions. The GAM shows $\delta^{13}C_{bel}$ decreasing from the Toarcian to the Middle Jurassic (Fig. 4). There is an increase into the Callovian, with the GAM dropping down again in the Upper Jurassic (Fig. 4). However, the data are sparse and fairly scattered in the Upper Jurassic and lower resolution variations may have been missed.

4. Discussion

4.1. Preservation

The preservation of the belemnite rostra was evaluated for any post-burial and/or meteoric diagenesis. Isotope ratios, element concentrations and ultra-structure examination collectively indicate whether the degree of preservation of the belemnites is pristine or if post-depositional overprinting biased them significantly (e.g. Ullmann and Korte, 2015; Ullmann et al., 2015). Decreasing Sr/Ca ratios, increasing Mn/Ca and Fe/Ca ratios and negative correlation between $\delta^{13}C$ and $\delta^{18}O$ (Brand and Veizer, 1980, 1981; Veizer, 1983; Marshall, 1992; Nunn et al., 2009; Nunn and Price, 2010; Ullmann and Korte, 2015; Ullmann et al., 2015) are common indicators for diagenetic alteration in belemnite rostra. Comparison of the "well-preserved" belemnite rostral data to the data from the apical line sub-samples helps to distinguish diagenetic trends (Fig. 3), as this central porous part of the rostrum is rapidly infilled with diagenetic minerals after deposition, including diagenetic calcite phases. For the present study, the upper limit for Mn/Ca ratio is conservatively placed at 0.15 mmol/mol, based on where apical line values dominate the signal (Fig. 3D), comparable to literature Mn/Ca limits between 0.06 and 0.46 mmol/mol for well-preserved Jurassic belemnites (e.g. Ullmann and Korte, 2015). An upper limit for Fe is placed at 2 mmol/mol (Fig. 3D).

The $\delta^{18}O_{bel}$ and $\delta^{13}C_{bel}$ show a slight negative correlation (Fig. 3A), with r^2 values of 0.41 for the apical line samples and 0.26 for the rostrum samples. We place a limit of −5‰ on $\delta^{18}O_{bel}$ for rostrum to be considered in the compiled data since apical line values dominate below this (Fig. 3A).

Decreasing strontium incorporation into the calcite may also be an indicator of diagenesis, yet it is also related to the growth rate (whereby fast precipitation results in Sr enrichment), and the amount present in the seawater (Lorens, 1981; Shen et al., 2001; Ullmann et al., 2013b; Ullmann and Korte, 2015; Korte et al., 2017). Likewise, the Sr/Ca ratio of seawater can be affected by seawater temperature resulting in higher concentrations with increasing temperatures (Dodd, 1965; Korte and

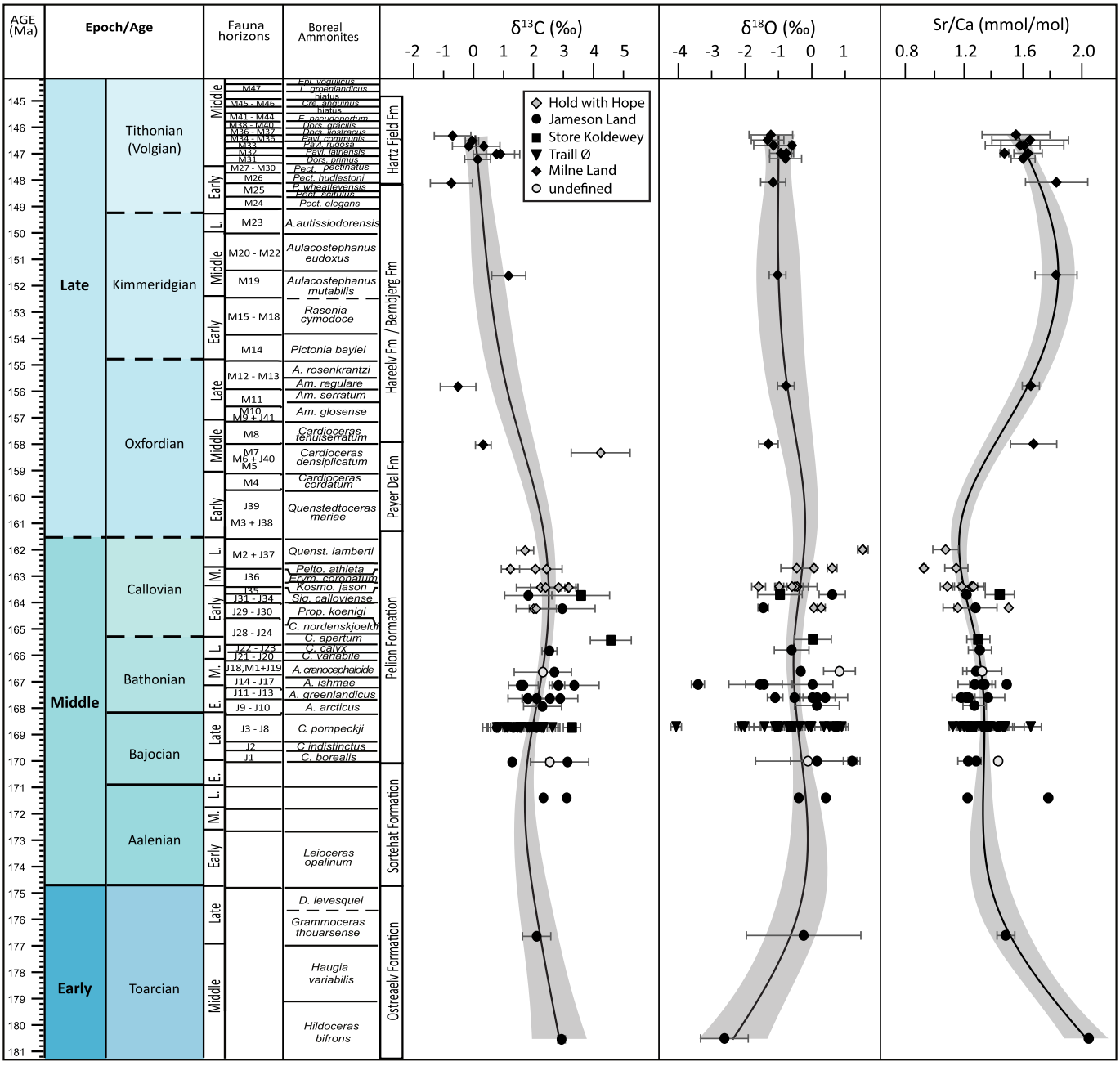

Fig. 4. Belemnite $\delta^{18}O$ and $\delta^{13}C$ values and Sr/Ca ratios from this study plotted against Subboreal ammonite stratigraphy and relative sea level (Surlyk, 2003). The belemnite data are binned according to their Subboreal ammonite zone (due to the lithostratigraphic variation between outcrops making it impossible to plot the data against lithostratigraphic height). Each data point represents an average of the unaltered subsamples, and the error bars indicate the standard deviation.

Hesselbo, 2011). These other influences therefore complicate the interpretation of the Sr/Ca ratios; a vague positive correlation is observed between $\delta^{18}O_{bel}$ and Sr/Ca in apical line samples ($r^2 = 0.45$), suggesting a diagenetic trend, whereas the rostral samples show, if anything, increasing Sr/Ca with decreasing $\delta^{18}O_{bel}$ ($r^2 = 0.2$ excluding the 4 outliers; Fig. 3C). This may be related to temperature or changing seawater Sr/Ca (i.e. change in ocean current patterns), both of which may result in the observed covariance of Mg/Ca and $\delta^{18}O_{bel}$.

Magnesium incorporation into calcite may similarly be affected by growth rate, temperature, degree of alteration and seawater Mg/Ca values (Nunn and Price, 2010; Ries, 2010; Ullmann et al., 2015). As seawater Mg/Ca ratios are believed to have varied significantly throughout the Jurassic (e.g. Ries, 2010), and as a positive correlation between Mg/Ca and $\delta^{18}O_{bel}$ is most clear in the altered apical line samples (Fig. 3B; Ullmann et al., 2015), we do not consider that precipitation temperature was the main control on Mg/Ca of the belemnite rostra analysed.

4.2. Effect of local processes on the stable isotope record

It is necessary to evaluate if local processes affected the belemnite stable isotope signal in the East Greenlandic basins, as the depositional environments across these basins were temporally and spatially variable (Fig. 5), which may have dampened or amplified the broader regional isotope trends along the Viking Corridor. Such effects may be responsible for the unusually heavy $\delta^{13}C$ values for the belemnite rostrum in the proximal shallow-marine sand at Store Koldewey (>3.5‰), compared to the other localities which represent more distal

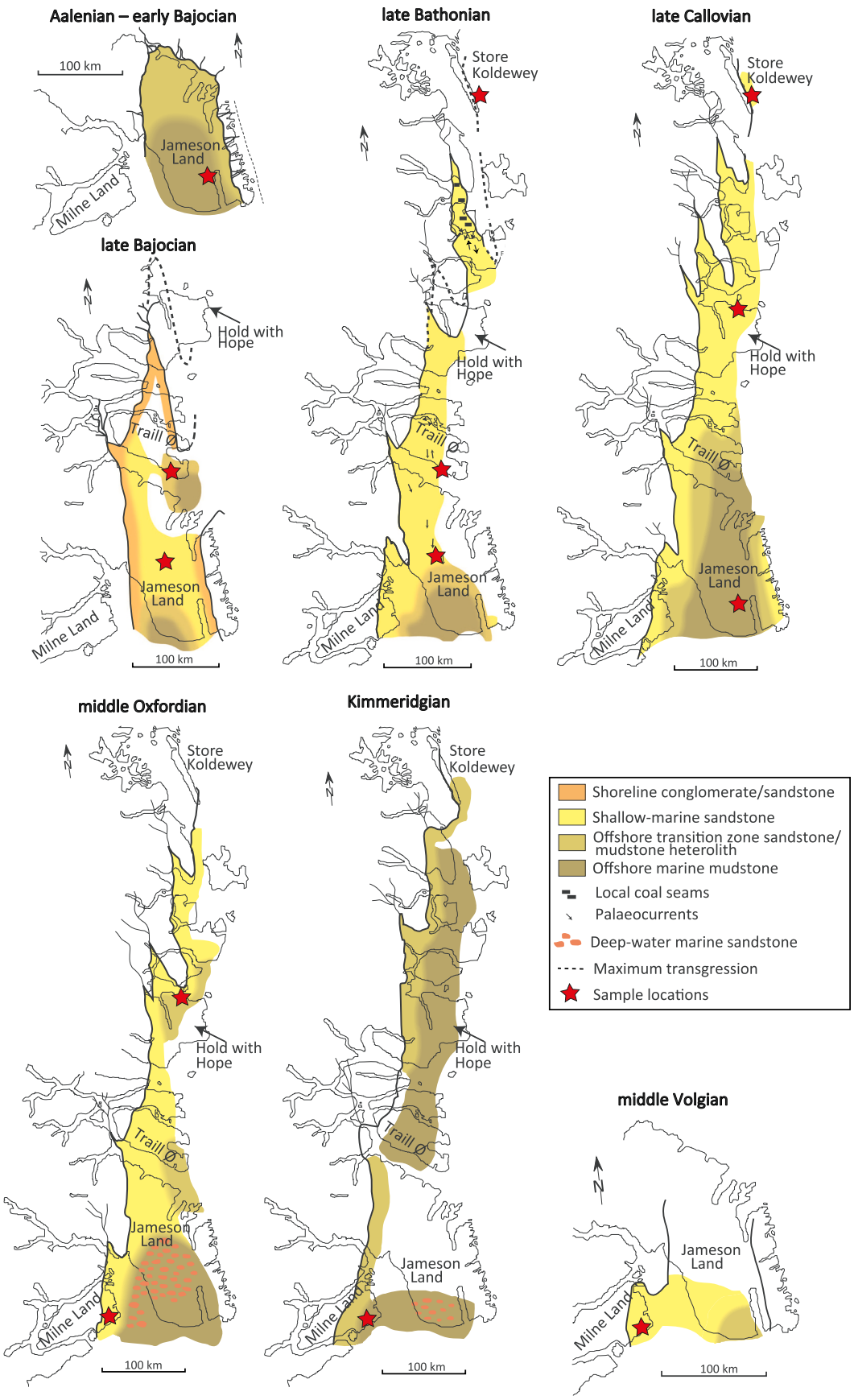

Fig. 5. Palaeogeographic evolution of East Greenland during the Middle and Late Jurassic showing the transgressive trend from the Aalenian to the early Volgian (Surlyk, 2003). Red stars mark location of belemnites from that interval. (For interpretation of the references to colour in this figure legend, the reader is referred to the web version of this article.)

environments (Fig. 4). The $\delta^{13}C$ signals may indicate that the water masses in the northern Wollaston Foreland Basin and the southern Jameson Land Basin were not fully connected. The $\delta^{13}C$ signal of the Wollaston Foreland Basin may predominantly have been influenced by water exchange from the Arctic Ocean with a heavier $\delta^{13}C$ composition compared to the dissolved inorganic carbon ratio ($\delta^{13}C_{DIC}$) of the southern Viking Corridor, which was connected to the Jameson Land Basin. Alternatively, spring blooming may have played a role in the $\delta^{13}C$ offset between the sections and possibly affecting the shallow areas more (e.g. Ullmann et al., 2013c). Previous authors have also suggested a strong lithological control on $\delta^{13}C_{carb}$ due to local variation in carbonate composition causing an offset between $\delta^{13}C_{carb}$ and $\delta^{13}C_{org}$ in a Lower Cretaceous succession of south-eastern France (Bodin et al., 2016). Erosion of the proposed late Early Jurassic doming in North-East Greenland (Surlyk, 1978) may also explain the offset in $\delta^{13}C$. The Bathonian–Callovian data fill a gap in the Subboreal and Boreal belemnite isotope record enabling comparison to coeval datasets (Fig. 6). Therefore, further investigation is needed to establish if the cause for this lateral variation in the Bathonian $\delta^{13}C$ signal is of local or regional extent.

4.3. Paleoceanographic and climatic trends

Both the $\delta^{18}O$ of the seawater from which a calcite grew ($\delta^{18}O_{sw}$),

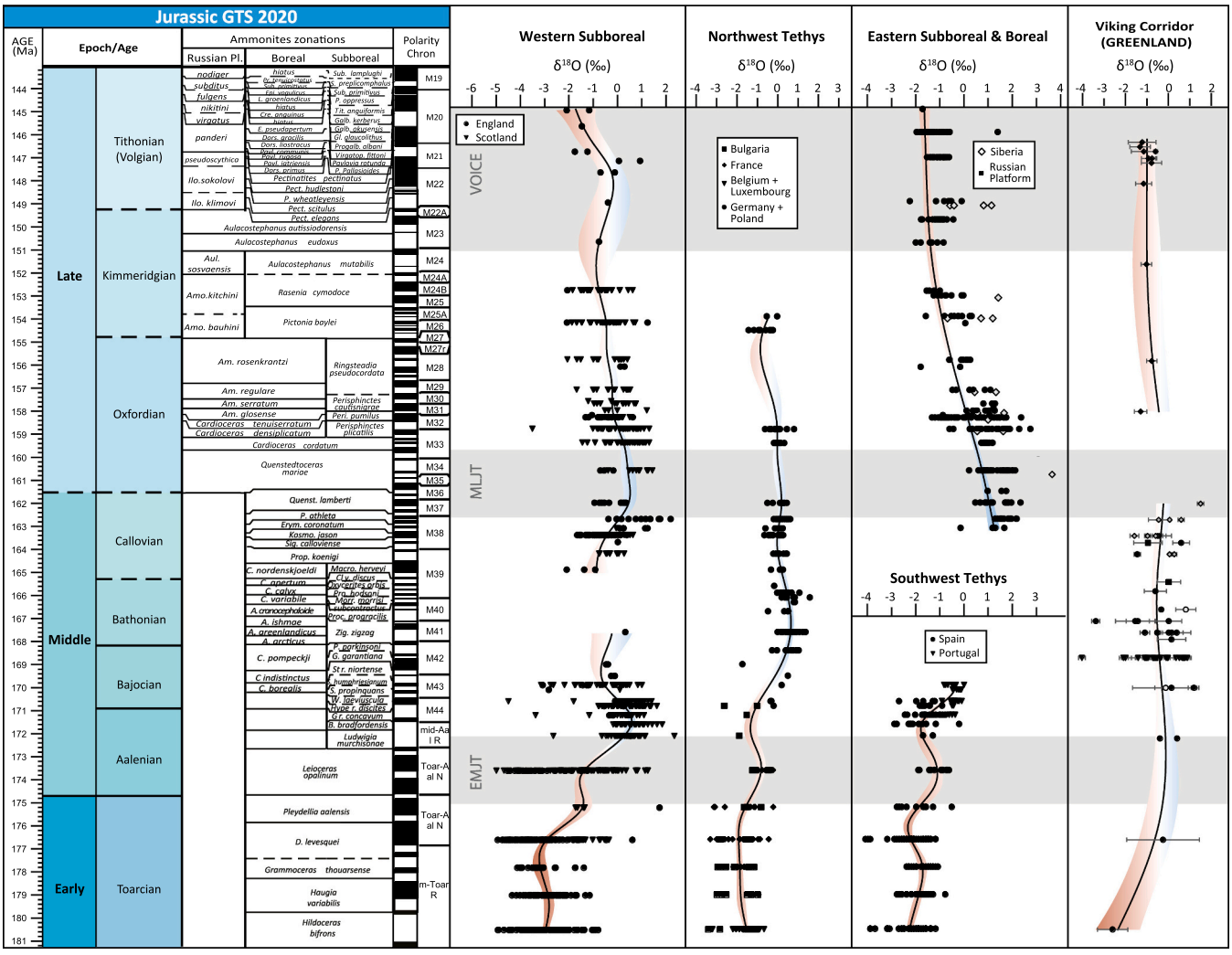

Fig. 6. Belemnite $\delta^{18}O$ trends across the Euro-Boreal region. Only belemnite $\delta^{18}O$ records are shown as it has been demonstrated that belemnites fractionate ^{18}O closer to equilibrium than other molluscs (e.g. brachiopods), and therefore direct comparison of belemnites with other molluscan $\delta^{18}O$ should not be undertaken (Bajnai et al., 2020; Vickers et al., 2021). The data have been binned by biozone (ammonite biostratigraphy), and are shown as points (shape related to locality – see key in figure). Correlation of ammonite zones between the Russian Platform, Boreal Realm and Subboreal Province is based on Rogov (2010) and Hesselbo et al. (2020). The black line is the general additive model fitted to the data (which is shown as points); the confidence interval is for the fit of the model given the data (further details for the GAM described in Section 2.4). This has been coloured red to blue to indicate that more negative $\delta^{18}O$ may reflect warmer conditions, and more positive values with cooler conditions. However, as discussed in the text, $\delta^{18}O_{bel}$ is not a direct temperature measurement as other factors affect the $\delta^{18}O$ of belemnites. Data from northern Siberia (Boreal Realm) is shown as the data points only on top of the eastern Subboreal Province data, as they are so few; the Siberia data was not included in the GAM for the eastern Subboreal Province. Data was compiled for the subregions from the following publications: Western Subboreal Province from Anderson et al. (1994); McArthur et al. (2000); Jenkyns et al. (2002); Wierzbowski (2002, 2004); Price and Page (2008); Nunn et al. (2009); Price (2010); Li et al. (2012); Ullmann et al. (2014); and Korte et al. (2015). Northwest Tethys from Podlaha et al. (1998); Wierzbowski (2002, 2004), Wierzbowski et al., 2009, Wierzbowski and Joachimski (2007); Metodiev and Koleva-Rekalova (2008); Dera et al. (2009b); Korte et al. (2015). Southwest Tethys from Jenkyns et al. (2002); van de Schootbrugge et al. (2005); Gómez et al. (2008, 2009). Eastern Subboreal Province from Podlaha et al. (1998); Riboulleau (2000); Riboulleau et al. (1998); Gröcke et al. (2003); Price and Rogov (2009); Žák et al. (2011); Wierzbowski et al. (2013); Wierzbowski and Rogov (2011). (For interpretation of the references to colour in this figure legend, the reader is referred to the web version of this article.)

and the temperature at which it was precipitated, are known to affect its $\delta^{18}O$ (e.g., Anderson and Arthur, 1983). For this reason, we have not converted raw $\delta^{18}O_{bel}$ to temperature as this requires making assumptions regarding the $\delta^{18}O_{sw}$ which cannot be justified (e.g. Wierzbowski et al., 2018). During the Middle and Late Jurassic, the Euro-Boreal region (consisting of the Boreal Realm, Subboreal Province and Tethys Realm) was comprised of a series of semi-restricted basins (Fig. 1). As such, these basins are likely to have experienced strong changes in salinity, linked to changes in paleocurrent directions and climate-related changes in the hydrological cycle, all of which could lead to a local $\delta^{18}O_{sw}$ value different from the global average (e.g. Zhou et al., 2008). The possibility of the waxing and waning of small polar ice-caps (as proposed by Dromart et al., 2003) would further exacerbate this effect as it pushes the global average $\delta^{18}O_{sw}$ to lower values (e.g. Shackleton and Kennett, 1975). Recent clumped isotopic studies demonstrate that a broad range in $\delta^{18}O_{sw}$ (>3‰) is recorded by belemnites from a single biozone at a single location (Vickers et al., 2021) and across high to low latitudes in a single time slice (Price et al., 2020), and that a broader range (>6‰) is observed at a one locality over geological time (e.g. Middle to Late Jurassic or Late Jurassic to Early Cretaceous; Wierzbowski et al., 2018; Vickers et al., 2019, 2020). Thus, in order to untangle the climatic palaeoceanographic signals in the Euro-boreal region during the Middle and Late Jurassic, intercomparison of different regions/basins is necessary, along with other, independent temperature proxy and palaeogeographic-indicative data.

The end of the Early Jurassic saw the most extreme changes in climate, carbon cycling and oceanography of the entire Jurassic period, during the Toarcian Ocean Anoxic Event (TOAE). This global event resulted in a second-order mass-extinction due to the combination of warm climate and low oxygen conditions in the ocean, and is characterised by a large excursion in organic and carbonate carbon isotope records, and multiple perturbations in marine carbonate $\delta^{18}O$ records (e.g. Jenkyns, 2010; Danise et al., 2013; Ullmann et al., 2020; Rübsam et al., 2020). The TOAE carbon isotope event peaked in the lower Toarcian (*falciferum* zone) and carbon records had returned to pre-CIE values by the *bifrons* zone (e.g. Suan et al., 2015; Hougård et al., 2021). Belemnite and bivalve $\delta^{18}O$ records from southwest Tethys across the CIE itself generally covary with biomarker SSTs, yet the $\delta^{18}O$ records are observed to show greater variability, likely due to the effect of varying $\delta^{18}O_{sw}$ as well as climate (Rübsam et al., 2020). Clay mineral distributions indicate variable climate (warm humid and cool dry) across the Toarcian, with the late Toarcian being characterised by cooler, drier climate than the middle Toarcian (Dera et al., 2009a). From the peak of the negative CIE into the Middle Jurassic, belemnite oxygen isotope records show variability across different regions (Fig. 6). In the northern U.K., $\delta^{18}O_{bel}$ remaining low until the Toarcian-Aalenian boundary (Fig. 6; Korte et al., 2015). Doré (1991) and Korte et al. (2015) hypothesised that the isotopic trends observed in the northern U.K. were due to northward transport of warm seawater impeded by doming in the North Sea, which had triggered regional cool-mode conditions as heat transport to the Arctic ceased. This barrier may have caused the observed separation of the Boreal faunas from the Tethyan faunas (Doré, 1991; see also Meledina et al., 2005). In the northwest and southwest Tethys, there is a decrease (i.e. warming/freshening) in $\delta^{18}O_{bel}$ at the Toarcian–Aalenian boundary (*aalensis* zone), with a positive peak (consistent with cooling) occurring later (in the lowest Aalenian *opalinum* zone) (Fig. 6). Yet, offset in peak cooling may be an artefact of data treatment; by binning of the data by biozone it is difficult to assess if the Tethys Realm truly saw a delay in the cooling compared to the western Subboreal Province. Due to the sparse sampling across the Toarcian interval in Greenland, trends in the Viking corridor are difficult to pick out, though it is noted that lowest (i.e. warmest/freshest) $\delta^{18}O$ values for the whole study are observed in the Toarcian compared to the Middle and Upper Jurassic. A lack of data from the Aalenian mean it is not possible to determine where $\delta^{18}O$ began to increase; high ("cooler") $\delta^{18}O_{bel}$ is observed in the Bajocian, where the first Middle Jurassic samples were measured.

Recent carbon isotope work has suggested that global atmospheric pCO_2 experienced at least two low interludes during the early Bajocian (in the *Propinquans* and *Humphriesianum* zones), with the possibility of the development of transient continental ice-caps as suggested by the coincidence of relative sea-level fluctuations with $\Delta^{13}C$ records (Bodin et al., 2020). Whilst our stable isotope data and comparison with other records, binned as they are by biozone, cannot resolve biozone-scale and higher resolution trends, the western Subboreal Province does show a positive peak (consistent with cooling/ increased salinity) in the across the Aalenian – Bajocian boundary, and in the southwest Tethys a positive peak is observed in earliest Bajocian (Fig. 6). These peaks, and the heavier $\delta^{18}O_{bel}$ observed in Greenland are consistent with Bajocian cooling and ice-cap development (which would have removed ^{16}O from the ocean system). The $\delta^{13}C_{bel}$ records show much scatter in the western Subboreal province, making the signal difficult to interpret (again, this may be an artefact of the data treatment, with the "bins" being too broad to identify higher resolution trends), yet small positive peaks in $\delta^{13}C_{bel}$ south- and northwest Tethys are consistent with lower atmospheric CO_2 (Fig. 7).

The Bathonian and Callovian saw Tethyan ammonite migration poleward (Poulsen and Riding, 2003), which ultimately resulted in a full ammonite faunal reconnection by the Callovian (Doré, 1991; Torsvik et al., 2002; Callomon, 2003; Page, 2008). This was coincident with an overall transgressive trend of the Middle Jurassic succession in East Greenland (Poulsen and Riding, 2003). The Subboreal Province records do not span this interval, yet in the northwest Tethys, higher ("cooler" or more saline) values persist through the Bathonian and Callovian, although are slightly higher in the Bathonian than Callovian (Fig. 6). The Viking Corridor maintains a fairly constant average $\delta^{18}O_{bel}$ throughout this interval; slightly lower in the Bathonian than the Callovian. By the observed northward migration of Tethyan ammonites, we would expect that northwards (i.e. Tethys-sourced) currents became more dominant during this this interval the Viking Corridor. Therefore, the low-amplitude trend to higher values in the Callovian, and the overall high $\delta^{18}O_{bel}$ values in northwest Tethys may reflect salinity changes rather than temperature.

A cool episode of c. 1–3 °C spanning the Callovian – Oxfordian boundary was proposed by Dromart et al. (2003), based on floral and faunal assemblages and $\delta^{18}O$ of shark tooth enamel from northwest Tethys. An invasion of Boreal ammonites southwards through the Callovian-Oxfordian boundary interval, and changes in palynofloral assemblages, are consistent with cooler, humid conditions during this time (Poulsen and Riding, 2003; Dromart et al., 2003 and references therein). As data from Greenland are lacking across this interval, it is not possible to assess trends along the Viking corridor spanning the Callovian – Oxfordian boundary, yet we note that the highest belemnite value measured for the Viking Corridor is measured in the *lamberti* zone. Belemnite $\delta^{18}O$ data from western and eastern Subboreal Province show a positive $\delta^{18}O_{bel}$ peak (consistent with cooling) across the Callovian-Oxfordian boundary (Fig. 6); Both show highest values in the *athleta* zone. A much smaller magnitude peak is observed in the northwest Tethys, but we note that there is a lack of data for the *mariae* zone. The trends to higher ("cooler") $\delta^{18}O_{bel}$ with a larger magnitude change in the Subboreal Province than northwest Tethys are consistent with a change in oceanography bringing cold, Boreal waters southward during the Callovian – Oxfordian transition (Fig. 6).

A gentle decreasing in $\delta^{18}O_{bel}$ (i.e. "warming") is apparent from the middle Oxfordian to the upper Kimmeridgian in both western and eastern Subboreal Provinces, and is more pronounced in the Russian Platform (Fig. 6). However, belemnite clumped isotope temperature reconstructions for the Russian Platform reveal an almost invariable belemnite calcite temperature throughout the Late Jurassic, suggesting that the $\delta^{18}O_{bel}$ trends were largely driven by a decrease in salinity on the Russian Platform, rather than changes in temperature (Wierzbowski et al., 2018). Yet, the large error (often $> \pm 5$ °C) and low resolution of

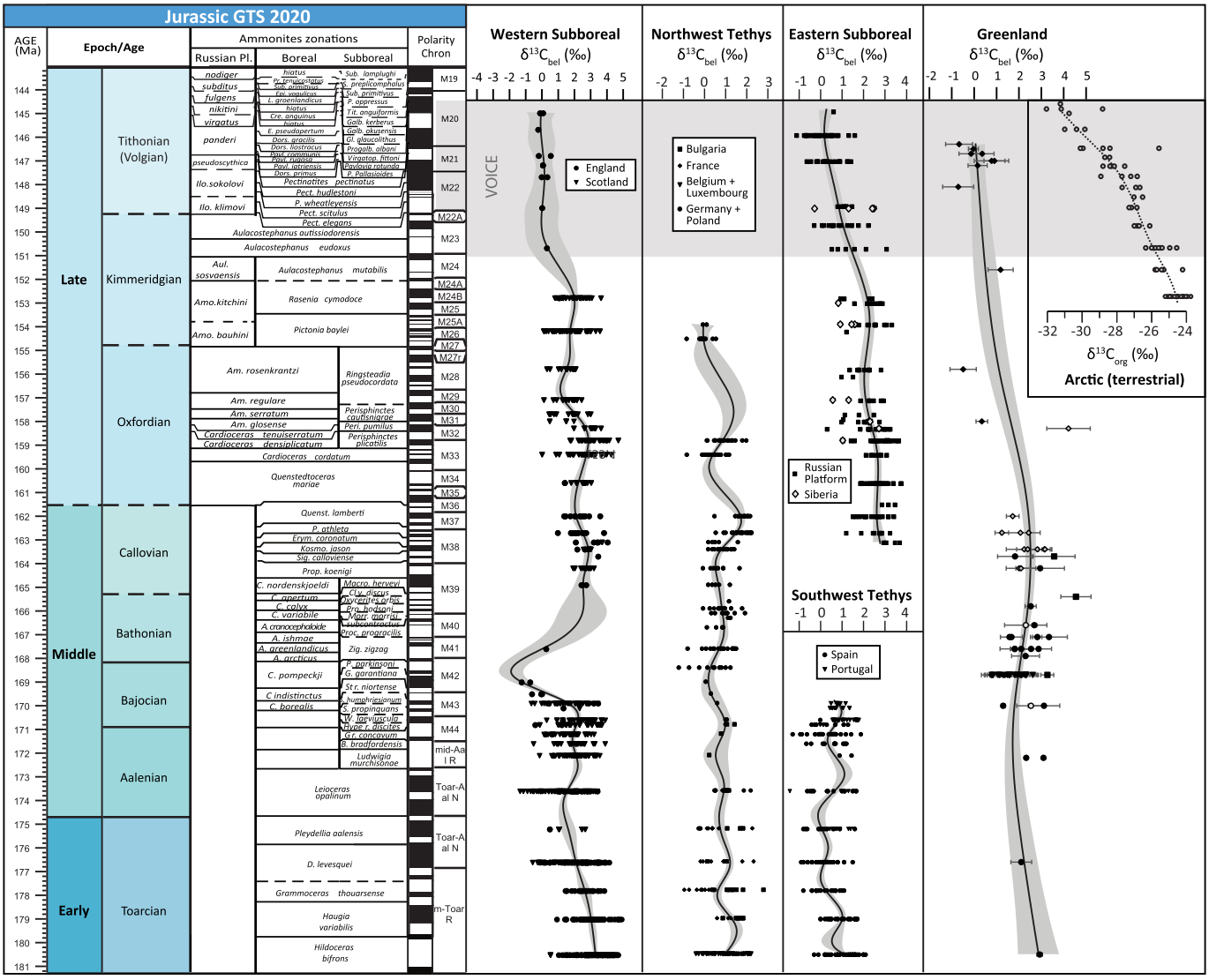

Fig. 7. Belemnite $\delta^{13}C$ trends across the Euro-Boreal region. Data, data treatment, and timescale as given in Fig. 6, except for the addition of $\delta^{13}C_{org}$ data from Arctic Svalbard (Koevoets et al., 2016; Koevoets et al., 2018 and Jelby et al., 2020), showing the declining limb of the VOICE event (dotted trendline fitted by eye).

the clumped isotopic study means that smaller magnitude (e.g. 1–3 °C) changes in temperature may not have been resolved. Independent of $\delta^{18}O_{bel}$, Boreal ammonite forms retreated northwards in the middle Oxfordian and Tethyan forms dominated European assemblages (Dromart et al., 2003 and references therein). Greenland belemnite data (Viking Corridor) are sparse across this interval, yet an increasing trend is observed starting from the *corontaum* zone and into the *lamberti* zone. In the upper Oxfordian to upper Kimmeridgian, Greenland belemnites maintain an average $\delta^{18}O_{bel}$ of c. -1‰, with no significant departures to higher or lower values, although data are too sparse through this interval to determine if this is significant. This co-varying $\delta^{18}O_{bel}$ trend across the Subboreal Province, and the evidence of co-occurring ammonite fauna between Greenland, the North Sea and the Russian Platform may suggest that the seaway remained open during the Oxfordian and lower – middle Kimmeridgian (e.g. as suggested by Callomon, 1975; Callomon and Birkelund, 1982; Fig. 1) and that northward-flowing currents became more dominant (Fig. 6). This is supported by the sparse data from northern Siberia which shows similar $\delta^{18}O_{bel}$ values to the Russian Platform in the Oxfordian, but becoming increasingly offset (more positive) than the Russian Platform in the Kimmeridgian (Fig. 6).

In the upper Kimmeridgian, Arctic organic carbon isotope ($\delta^{13}C_{org}$) records evolve away from global records, showing a distinct negative excursion of magnitude of 3–5‰ which peaks in the Volgian (upper Tithonian), and is known as the 'Volgian Isotopic Carbon Excursion' (VOICE) event (e.g. Hammer et al., 2012; Koevoets et al., 2016; Galloway et al., 2020; Jelby et al., 2020). Subboreal $\delta^{13}C_{org}$ records also show a decreasing trend, although not as distinctive as the high Arctic records from Canada and Svalbard (Fig. 7; Jelby et al., 2020). Whilst belemnite $\delta^{13}C$ records show more scatter than sedimentary organic matter records, a declining trend is observed in the Subboreal Province and suggested by the sparse data from Greenland (Fig. 7). Faulting in the North Sea and/or eustatic sea-level fall are believed to have caused an oceanographic barrier that separated the relatively shallow epeiric seas of the high latitudes and the Arctic from the open oceans of the Tethys (Doré, 1991). This led to significant faunal differences between Greenland and England in middle Tithonian times (Callomon and Birkelund, 1982; Birkelund and Callomon, 1985; Wierzbowski, 1989). Boreal ammonites became isolated and there was provincialism in dinoflagellate cysts in the Boreal and Tethys realms (Poulsen and Riding, 2003).

Yet, the cause of the VOICE negative CIE in high palaeolatitudes is still not understood. Eustatic sea-level fall and corresponding isolation of the Boreal Realm and Subboreal Province from the Tethys Realm is

hypothesised to have led to enhanced oxidation of organic matter (Galloway et al., 2020; Jelby et al., 2020). Observed black shale deposition in the Boreal Realm and Subboreal Province, which peaked during the Kimmeridgian and Volgian (Rogov et al., 2020), is consistent with stratification-prone slower circulation patterns leading to increased dysoxia-anoxia episodes in the shallow shelf seas of the Boreal realm, yet may be expected to have driven $\delta^{13}C_{sw}$ to more positive values. Georgiev et al. (2017) and Rogov et al. (2020) and hypothesise that long term warming accompanied this black shale deposition (as suggested by palynological and clay mineral data for the Boreal Realm); $\delta^{18}O_{bel}$ from the eastern and western Subboreal Province generally show a decreasing trend throughout the VOICE interval (Fig. 6). The style of black shale deposition in the Boreal realm at this time is quite different from typical OAEs, being limited to the Arctic/Boreal realm, diachronous across different basins and sub-basins, and with no significant faunal turnover (Rogov et al., 2020), and further work is needed to understand the mechanisms driving the observed changes in total organic matter content (black shales) and $\delta^{13}C$ in the northern high latitudes across the Jurassic-Cretaceous boundary (see global correlation of Upper Jurassic – Lower Cretaceous carbon-isotope records in Jelby et al., 2020).

5. Conclusions

Carbon-isotope and oxygen-isotope signals from well-preserved, East Greenlandic belemnites of Middle to Late Jurassic age are interpreted as representing the primary geochemical signal of palaeo-seawater, allowing comparison to other Euro-Boreal records. This enables some inferences to be made about changes in palaeoceanography and climate in this region. All records show an increase in $\delta^{18}O_{bel}$ values, consistent with cooling, after the Toarcian, although this may occurs earlier in the western Subboreal Province than in the northwest Tethys. The Middle to Late Jurassic transition is characterised by more positive (consistent with cooling) $\delta^{18}O_{bel}$ values from Subboreal Province, which, together with ammonite faunal distribution patterns, suggest a strengthening of southward-flowing cold currents from the Boreal Realm into the Subboreal Province. The uppermost Jurassic (Kimmeridgian and Tithonian/Volgian) see increases in both $\delta^{18}O_{bel}$ and $\delta^{13}C_{bel}$ in the Boreal Realm and Subboreal Province, consistent with the isolation of the Boreal Realm from the lower latitudes during this time, although the mechanisms of the drivers of these trends are not fully understood.

Declaration of Competing Interest

The authors declare that they have no known competing financial interests or personal relationships that could have appeared to influence the work reported in this paper.

Acknowledgements

We thank Michael Engkilde for access to his belemnite collection. These belemnites were primarily collected by M. Engkilde and J. Callomon in field seasons 1992-1994 and 1995-1998 on Jameson Land. The belemnites were collected from layers along with co-existing ammonites, which were subsequently determined by J. Callomon. A few belemnites, age-determined by co-existing ammonites, were collected by F. Surlyk, G. Dam, M. Larsen, H. Vosgerau, who all participated in the integrated field work in East Greenland in the 1990s. Other belemnites come from the Geological Museum of Denmarks's collection (M. Engkilde and J. Callomon). We acknowledge Bo Petersen for stable-isotope measurements and Jesper A. Frederiksen for preparing sample material for isotope analysis. The Danish Council for Independent Research–Natural Sciences (project DFF - 7014-00142 to CK) is acknowledged for funding this project. Funding for this study was also granted by the European Commission, Horizon 2020 Marie Skłodowska-Curie Actions (ICECAP; grant no. 101024218, to MLV), and by the Research Council of Norway through the Centres of Excellence funding scheme, project number 223272. MEJ acknowledges the Danish Offshore Technology Centre (DTU Offshore for financially supporting his postdoctoral research during which this work was partly carried out. We thank our reviewers, Stephane Bodin and an anonymous, for their constructive reviews.

Appendix A. Supplementary data

Supplementary data to this article can be found online at https://doi.org/10.1016/j.palaeo.2022.111014.

References

Alberti, M., Fürsich, F.T., Pandey, D.K., Ramkumar, M., 2012. Stable isotope analyses of belemnites from the Kachchh Basin, western India: paleoclimatic implications for the Middle to late Jurassic transition. Facies 58, 261–278.

Alsen, P., Piasecki, S., 2018. Biostratigraphy of the Hareelv Formation (Upper Jurassic) in the Blokelv-1 core, Jameson Land, central East Greenland. In: Ineson, J.R., Bojesen-Koefoed, J.A. (Eds.), Petroleum geology of the Upper Jurassic – Lower Cretaceous of East and North-East Greenland: Blokelv-1 borehole, Jameson Land Basin. Geological Survey of Denmark and Greenland Bulletin, *42*, pp. 15–37. https://doi.org/10.34194/geusb.v42.4308.

Anderson, T.F., Arthur, M.A., 1983. Stable isotopes in sedimentary geology and their application to sedimentologic and paleoenvironmental problems. In: Arthur, M.A., et al. (Eds.), Society of Economic Paleontologists and Mineralogists Short Course Notes, 10. SEPM, pp. 1–151.

Anderson, T.F., Popp, B.N., Williams, A.C., Ho, L.Z., Hudson, J.D., 1994. The stable isotopic records of fossils from the Peterborough Member, Oxford Clay Formation (Jurassic), UK: palaeoenvironmental implications. J. Geol. Soc. 151 (1), 125–138. https://doi.org/10.1144/gsjgs.151.1.0125.

Bajnai, D., Guo, W., Spötl, C., Coplen, T.B., Methner, K., Löffler, N., Krsnik, E., Gischler, E., Hansen, M., Henkel, D., Price, G.D., 2020. Dual clumped isotope thermometry resolves kinetic biases in carbonate formation temperatures. Nat. Commun. 11 (1), 1–9. https://doi.org/10.1038/s41467-020-17501-0.

Birkelund, T., Callomon, J.H., 1985. The Kimmeridgian ammonites faunas of Milne Land, central East Greenland. Bull. Grønl. Geol. Unders. 153, 56. https://doi.org/10.34194/bullggu.v153.6695.

Birkelund, T., Callomon, J.H., Fürsich, F.T., 1984. The stratigraphy of the Upper Jurassic and lower cretaceous sediments of Milne Land, central East Greenland. Bull. Grønl. Geol. Unders. 147, 56. https://doi.org/10.34194/bullggu.v147.6689.

Bodin, S., Krencker, F.-N., Kothe, T., Hoffmann, R., Mattioli, E., Heimhofer, U., Kabiri, L., 2016. Perturbation of the carbon cycle during the late Pliensbachian–early Toarcian: New insight from high-resolution carbon isotope records in Morocco. J. Afr. Earth Sci. 116, 89–104. https://doi.org/10.1016/j.jafrearsci.2015.12.018.

Bodin, S., Mau, M., Sadki, D., Danisch, J., Nutz, A., Krencker, F.-N., Kabiri, L., 2020. Transient and secular changes in global carbon cycling during the early Bajocian event: evidence for Jurassic cool climate episodes. Glob. Planet. Chang. 194, 103287 https://doi.org/10.1016/j.gloplacha.2020.103287.

Brand, U., Veizer, J., 1980. Chemical diagenesis of a multicomponent carbonate system; 1, Trace elements. J. Sediment. Res. 50 (4), 1219–1236. https://doi.org/10.1306/212f7bb7-2b24-11d7-8648000102c1865d.

Brand, U., Veizer, J., 1981. Chemical diagenesis of a multicomponent carbonate system; 2, Stable isotopes. J. Sediment. Res. 51 (3), 987–997. https://doi.org/10.1306/212f7df6-2b24-11d7-8648000102c1865d.

Callomon, J.H., 1975. Jurassic ammonites from the northern North Sea. Nor. Geol. Tidsskr. 55, 373–386.

Callomon, J.H., 1993. The ammonite succession in the Middle Jurassic of East Greenland. Bull. Geol. Soc. Den. 40, 83–113. https://doi.org/10.37570/bgsd-1994-40-03.

Callomon, J.H., 2003. The Middle Jurassic of western and northern Europe: its subdivisions, geochronology and correlations. Geol. Survey Denmark Greenland (GEUS) Bull. 1, 61–73. https://doi.org/10.34194/geusb.v1.4648.

Callomon, J.H., Birkelund, T., 1980. The Jurassic transgression and the mid-late Jurassic succession in Milne Land, central East Greenland. Geol. Mag. 117 (3), 211–226. https://doi.org/10.1017/s0016756800030442.

Callomon, J.H., Birkelund, T., 1982. The ammonite zones of the Boreal Volgian (Upper Jurassic) in East Greenland. In: Embry, A.F., Balkwill, H.R. (Eds.), Arctic Geology and Geophysics. Canadian Society of Petroleum Geologists Memoir, vol. 8, pp. 349–369.

Callomon, J.H., Alsen, P., Surlyk, F., 2015. The ammonites of the Middle Jurassic Cranocephalites beds of East Greenland. Geol. Survey Denmark Greenland Bull. 34, 1–127. https://doi.org/10.34194/geusb.v34.4488.

Danise, S., Twitchett, R.J., Little, C.T., Clemence, M.E., 2013. The impact of global warming and anoxia on marine benthic community dynamics: an example from the Toarcian (early Jurassic). PLoS One 8 (2), e56255. https://doi.org/10.1371/journal.pone.0056255.

Dera, G., Pellenard, P., Neige, P., Deconinck, J.-F., Pucéat, E., Dommergues, J.-L., 2009a. Distribution of clay minerals in early Jurassic Peritethyan seas: Palaeoclimatic significance inferred from multiproxy comparisons. Palaeogeogr. Palaeoclimatol. Palaeoecol. 271, 39–51. https://doi.org/10.1016/j.palaeo.2008.09.010.

Dera, G., Pucéat, E., Pellenard, P., Neige, P., Delsate, D., Joachimski, M.M., Reisberg, L., Martinez, M., 2009b. Water mass exchange and variations in seawater temperature

in the NW Tethys during the early Jurassic: Evidence from neodymium and oxygen isotopes of fish teeth and belemnites. Earth Planet. Sci. Lett. 286, 198–207. https://doi.org/10.1016/j.epsl.2009.06.027.
Dera, G., Brigaud, B., Monna, F., Laffont, R., Pucéat, E., Deconinck, J.F., Pellenard, P., Joachimski, M.M., Durlet, C., 2011. Climatic ups and downs in a disturbed Jurassic world. Geology 39 (3), 215–218. https://doi.org/10.1130/G31579.1.
Dodd, J.R., 1965. Environmental control of strontium and magnesium in Mytilus. Geochim. Cosmochim. Acta 29 (5), 385–398. https://doi.org/10.1016/0016-7037(65)90035-9.
Doré, A., 1991. The structural foundation and evolution of Mesozoic seaways between Europe and the Arctic. Palaeogeogr. Palaeoclimatol. Palaeoecol. 87 (1–4), 441–492. https://doi.org/10.1016/0031-0182(91)90144-g.
Doyle, P., 1987. Lower Jurassic-lower cretaceous belemnite biogeography and the development of the Mesozoic Boreal Realm. Palaeogeogr. Palaeoclimatol. Palaeoecol. 61, 237–254. https://doi.org/10.1016/0031-0182(87)90052-6.
Dromart, G., Garcia, J.-P., Picard, S., Atrops, F., Lecuyer, C., Sheppard, S.M.F., 2003. Ice age at the Middle-Late Jurassic transition? Earth Planet. Sci. Lett. 213, 205–220. https://doi.org/10.1016/S0012-821X(03)00287-5.
Dutton, A., Huber, B.T., Lohmann, K.C., Zinsmeister, W.J., 2007. High-resolution stable isotope profiles of a dimitobelid belemnite: implications for paleodepth habitat and late Maastrichtian climate seasonality. Palaios 22, 642–650.
Galloway, J.M., Vickers, M.L., Price, G.D., Poulton, T., Grasby, S.E., Hadlari, T., Beauchamp, B., Sulphur, K., 2020. Finding the VOICE: organic carbon isotope chemostratigraphy of Late Jurassic–Early Cretaceous Arctic Canada. Geol. Mag. 157 (10), 1643–1657. https://doi.org/10.1017/s0016756819001316.
Georgiev, S.V., Stein, H.J., Hannah, J.L., Xu, G., Bingen, B., Weiss, H.M., 2017. Timing, duration, and causes for Late Jurassic–Early Cretaceous anoxia in the Barents Sea. Earth Planet. Sci. Lett. 461, 151–162. https://doi.org/10.1016/j.epsl.2016.12.035.
Gómez, J.J., Goy, A., Canales, M.L., 2008. Seawater temperature and carbon isotope variations in belemnites linked to mass extinction during the Toarcian (Early Jurassic) in central and northern Spain. Comparison with other European sections. Palaeogeogr. Palaeoclimatol. Palaeoecol. 258, 28–58. https://doi.org/10.1016/j.palaeo.2007.11.005.
Gómez, J.J., Canales, M.L., Ureta, S., Goy, A., 2009. Palaeoclimatic and biotic changes during the Aalenian (Middle Jurassic) at the southern Laurasian Seaway (Basque–Cantabrian Basin, northern Spain). Palaeogeogr. Palaeoclimatol. Palaeoecol. 275 (1–4), 14–27. https://doi.org/10.1016/j.palaeo.2009.01.009.
Gröcke, D.R., Price, G.D., Ruffell, A.H., Mutterlose, J., Baraboshkin, E., 2003. Isotopic evidence for late Jurassic–Early Cretaceous climate change. Palaeogeogr. Palaeoclimatol. Palaeoecol. 202 (1–2), 97–118. https://doi.org/10.1016/S0031-0182(03)00631-X.
Hammer, Ø., Collignon, M., Nakrem, H.A., 2012. Organic carbon isotope chemostratigraphy and cyclostratigraphy in the Volgian of Svalbard. Norwegian J. Geol./Norsk Geologisk Forening 92 (2–3), 103–112.
Hesselbo, S.P., Ogg, J.G., Ruhl, M., Hinnov, L.A., Huang, C.J., 2020. The Jurassic Period. In: Gradstein, F.M., Ogg, J.G., Schmitz, M.D., Ogg, G.M. (Eds.), Geologic Time Scale 2020. Elsevier, pp. 955–1021.
Hoffmann, R., Stevens, K., 2019. The palaeobiology of belemnites–foundation for the interpretation of rostrum geochemistry. Biol. Rev. 95, 94–123. https://doi.org/10.1111/brv.12557.
Hougård, I.W., Bojesen-Koefoed, J.A., Vickers, M., Ullmann, C.V., Bjerrum, C.J., Rizzi, M., Korte, C., 2021. Redox element record shows that environmental perturbations associated with the T-OAE were of longer duration than the carbon isotope record suggests–the Aubach section, SW Germany. Newsl. Stratigr. 54 (2), 229–246. https://doi.org/10.1127/nos/2020/0630.
Jelby, M.E., Śliwińska, K.K., Koevoets, M.J., Alsen, P., Vickers, M.L., Olaussen, S., Stemmerik, L., 2020. Arctic reappraisal of global carbon-cycle dynamics across the Jurassic–Cretaceous boundary and Valanginian Weissert Event. Palaeogeogr. Palaeoclimatol. Palaeoecol. 555, 109847 https://doi.org/10.1016/j.palaeo.2020.109847.
Jenkyns, H.C., 2010. Geochemistry of oceanic anoxic events. Geochem. Geophys. Geosyst. 11 (3) https://doi.org/10.1029/2009GC002788.
Jenkyns, H.C., Jones, C.E., Gröcke, D.R., Hesselbo, S.P., Parkinson, D.N., 2002. Chemostratigraphy of the Jurassic System: applications, limitations and implications for palaeoceanography. J. Geol. Soc. Lond. 159, 351–378. https://doi.org/10.1144/0016-764901-130.
Klug, C., Schweigert, G., Fuchs, D., Kruta, I., Tischlinger, H., 2016. Adaptations to squid-style high-speed swimming in Jurassic belemnitids. Biol. Lett. 12, 20150877. https://doi.org/10.1098/rsbl.2015.0877.
Koevoets, M., Abay, T., Hammer, Ø., Olaussen, S., 2016. High-resolution organic carbon–isotope stratigraphy of the Middle Jurassic–Lower Cretaceous Agardhfjellet Formation of central Spitsbergen, Svalbard. Palaeogeogr. Palaeoclimatol. Palaeoecol. 449, 266–274. https://doi.org/10.1016/j.palaeo.2016.02.029.
Koevoets, M.J., Hammer, Ø., Olaussen, S., Senger, K., Smelror, M., 2018. Integrating subsurface and outcrop data of the Middle Jurassic to Lower Cretaceous Agardhfjellet Formation in central Spitsbergen. Nor. J. Geol. 98, 219–252.
Koppelhus, E.B., Hansen, C.F., 2003. Palynostratigraphy and palaeoenvironment of the middle Jurassic Sortehat formation (Neill Klinter Group), Jameson land, East Greenland. Geol. Survey Denmark Greenland Bull. 1, 777–811. https://doi.org/10.34194/geusb.v1.4689.
Korte, C., Hesselbo, S.P., 2011. Shallow marine carbon and oxygen isotope and elemental records indicate icehouse-greenhouse cycles during the Early Jurassic. Paleoceanography 26 (4), PA4219. https://doi.org/10.1029/2011PA002160.
Korte, C., Hesselbo, S.P., Ullmann, C.V., Dietl, G., Ruhl, M., Schweigert, G., Thibault, N., 2015. Jurassic climate mode governed by ocean gateway. Nat. Commun. 6 (1), 1–7. https://doi.org/10.1038/ncomms10015.
Korte, C., Thibault, N., Ullmann, C.V., Clémence, M.-E., Mette, W., Olsen, T.K., Rizzi, M., Ruhl, M., 2017. Brachiopod biogeochemistry and isotope stratigraphy from the Rhaetian Eiberg section in Austria: potentials and limitations. Neues Jahrbuch für Geologie und Paläontologie-Abhandlungen 117-138. https://doi.org/10.1127/njgpa/2017/0651.
Li, Q., McArthur, J.M., Atkinson, T.C., 2012. Lower Jurassic belemnites as indicators of palaeo-temperature. Palaeogeogr. Palaeoclimatol. Palaeoecol. 315–316, 38–45. https://doi.org/10.1016/j.palaeo.2011.11.006.
Lorens, R.B., 1981. Sr, Cd, Mn and Co distribution coefficients in calcite as a function of calcite precipitation rate. Geochim. Cosmochim. Acta 45 (4), 553–561. https://doi.org/10.1016/0016-7037(81)90188-5.
Marshall, J.D., 1992. Climatic and oceanographic isotopic signals from the carbonate rock record and their preservation. Geol. Mag. 129 (2), 143–160. https://doi.org/10.1017/s0016756800008244.
McArthur, J., Donovan, D., Thirlwall, M., Fouke, B., Mattey, D., 2000. Strontium isotope profile of the early Toarcian (Jurassic) oceanic anoxic event, the duration of ammonite biozones, and belemnite palaeotemperatures. Earth Planet. Sci. Lett. 179 (2), 269–285. https://doi.org/10.1016/s0012-821x(00)00111-4.
Meledina, S.V., Shurygin, B.N., Dzyuba, O.S., 2005. Stages in development of mollusks, paleobiogeography of boreal seas in the Early-Middle Jurassic and zonal scales of Siberia. Russ. Geol. Geophys. 46 (3), 239–255.
Metodiev, L., Koleva-Rekalova, E., 2008. Stable isotope records (δ18O and δ13C) of Lower-Middle Jurassic belemnites from the western Balkan mountains (Bulgaria): Palaeoenvironmental application. Appl. Geochem. 23, 2845–2856. https://doi.org/10.1016/j.apgeochem.2008.04.010.
Milner, P.S., Piasecki, S., 1996. Boreal Middle Jurassic dinoflagellate cyst stratigraphy of Jameson Land, East Greenland. In: Piasecki, S., et al. (Eds.), Formation of Source and Reservoir Rocks in a Sequence Stratigraphic Framework, Jameson Land, East Greenland. Energy Research Programme EFP-93, Projects 1313/93 and 00171996/30, Vol. I and II. Danmarks og Grønlands Geologiske Undersøgelse Rapport, p. 46.
Nunn, E.V., Price, G.D., 2010. Late Jurassic (Kimmeridgian–Tithonian) stable isotopes (δ18O, δ13C) and Mg/Ca ratios: new palaeoclimate data from Helmsdale, Northeast Scotland. Palaeogeogr. Palaeoclimatol. Palaeoecol. 292 (1–2), 325–335. https://doi.org/10.1016/j.palaeo.2010.04.015.
Nunn, E.V., Price, G.D., Hart, M.B., Page, K.N., Leng, M.J., 2009. Isotopic signals from Callovian–Kimmeridgian (Middle–Upper Jurassic) belemnites and bulk organic carbon, Staffin Bay, Isle of Skye, Scotland. J. Geol. Soc. 166 (4), 633–641. https://doi.org/10.1144/0016-76492008-067.
Page, K.N., 2008. The evolution and geography of Jurassic ammonoids. Proc. Geol. Assoc. 119 (1), 35–57. https://doi.org/10.1016/s0016-7878(08)80257-x.
Piasecki, S., 1996. Boreal dinoflagellate cyst stratigraphy of Middle to Upper Jurassic sediments of Milne Land, East Greenland. In: Piasecki, S., et al. (Eds.), Formation of Source and Reservoir Rocks in a Sequence Stratigraphic Framework, Jameson Land, East Greenland. Energy Research Programme EFP-93, Projects 1313/93 and 00171996/30, Vol. I and II. Danmark og Grønlands Geologiske Undersøgelse Rapport, p. 100.
Piasecki, S., Stemmerik, L., 2004. Jurassic dinoflagellate cysts from Hochstetter Forland, North-East Greenland. Geol. Survey Denmark Greenland Bull. 5, 89–97. https://doi.org/10.34194/geusb.v5.4809.
Piasecki, S., Larsen, M., Jens Therkelsen, J., Vosgerau, H., 2004a. Jurassic dinoflagellate cyst stratigraphy of hold with Hope, North-East Greenland. Geol. Survey Denmark Greenland Bull. 5, 73–88. https://doi.org/10.34194/geusb.v5.4808.
Piasecki, S., Callomon, H.J., Stemmerik, L., 2004b. Jurassic dinoflagellate cyst stratigraphy of Store Koldewey, North-East Greenland. Geol. Survey Denmark Greenland Bull. 5, 99–112. https://doi.org/10.34194/geusb.v5.4810.
Podlaha, O.G., Mutterlose, J., Veizer, J., 1998. Preservation of δ18O and δ13C in belemnite rostra from the Jurassic/early cretaceous successions. Am. J. Sci. 298, 324–347. https://doi.org/10.2475/ajs.298.4.324.
Poulsen, N.E., Riding, J.B., 2003. The Jurassic dinoflagellate cyst zonation of subboreal Northwest Europe. Geol. Survey Denmark Greenland (GEUS) Bull. 1, 115–144. https://doi.org/10.34194/geusb.v1.4650.
Price, G.D., 2010. Carbon-isotope stratigraphy and temperature change during the Early–Middle Jurassic (Toarcian–Aalenian), Raasay, Scotland, UK. Palaeogeogr. Palaeoclimatol. Palaeoecol. 285 (3–4), 255–263. https://doi.org/10.1016/j.palaeo.2009.11.018.
Price, G.D., Page, K.N., 2008. A carbon and oxygen isotopic analysis of molluscan faunas from the Callovian–Oxfordian boundary at Redcliff Point, Weymouth, Dorset: implications for belemnite behaviour. Proc. Geol. Assoc. 119, 153–160. https://doi.org/10.1016/S0016-7878(08)80315-X.
Price, G.D., Rogov, M.A., 2009. An isotopic appraisal of the late Jurassic greenhouse phase in the Russian Platform. Palaeogeogr. Palaeoclimatol. Palaeoecol. 273 (1–2), 41–49. https://doi.org/10.1016/j.palaeo.2008.11.011.
Price, G.D., Bajnai, D., Fiebig, J., 2020. Carbonate clumped isotope evidence for latitudinal seawater temperature gradients and the oxygen isotope composition of early cretaceous seas. Palaeogeogr. Palaeoclimatol. Palaeoecol. 552, 109777 https://doi.org/10.1016/j.palaeo.2020.109777.
Riboulleau, A., 2000. Géochimie des black shales du jurassique supérieur de la plateforme russe. In: Processus de sédimentation de la matière organique. *PhD thesis*, Paris VI.
Riboulleau, A., Baudin, F., Deaux, V., Hantzpergue, P., Renard, M., Zakharov, V., 1998. Évolution de la paléotempérature de eaux de la plate-forme rusee au cours du Jurassique supérieur. Comp. Rendus de l'Acad. Sci. Série II 326, 239–246.
Ries, J.B., 2010. Geological and experimental evidence for secular variation in seawater Mg/Ca (calcite-aragonite seas) and its effects on marine biological calcification. Biogeosciences 7 (9), 2795–2849. https://doi.org/10.5194/bg-7-2795-2010.

Rogov, M., 2010. New data on ammonites and stratigraphy of the Volgian stage in Spitzbergen. Stratigr. Geol. Correl. 18 (5), 505–531. https://doi.org/10.1134/s0869593810050047.
Rogov, M., Shchepetova, E., Zakharov, V., 2020. Late Jurassic–earliest Cretaceous prolonged shelf dysoxic–anoxic event and its possible causes. Geol. Mag. 157 (10), 1622–1642. https://doi.org/10.1017/s001675682000076x.
Rübsam, W., Reolid, M., Sabatino, N., Masetti, D., Schwark, L., 2020. Molecular paleothermometry of the early Toarcian climate perturbation. Glob. Planet. Chang. 195, 103351.
Servén, D., Brummitt, C., 2018. pyGAM: Generalized Additive Models in Python. Zenodo. https://doi.org/10.5281/zenodo.1208723.
Shackleton, N., Kennett, J., 1975. Paleotemperature History of the Cenozoic and the Initiation of Antarctic Glaciation: Oxygen and Carbon Isotope Analyses in DSDP Sites 277, 279, and 281, vol. 29. US Government Printing Office.
Shen, C.-C., Hastings, D.W., Lee, T., Chiu, C.-H., Lee, M.-Y., Wei, K.-Y., Edwards, R.L., 2001. High precision glacial–interglacial benthic foraminiferal Sr/Ca records from the eastern equatorial Atlantic Ocean and Caribbean Sea. Earth Planet. Sci. Lett. 190 (3–4), 197–209. https://doi.org/10.1016/s0012-821x(01)00391-0.
Spath, L.F., 1932. The invertebrate faunas of the Bathonian-Callovian deposits of Jameson Land (East Greenland). Medd. Grønland 87 (7), 158.
Spath, L., 1935. The Upper Jurassic invertebrate faunas of Cape Leslie, Milne Land. l. Oxfordian and Lower Kimmeridgian. Medd. Grønland 99 (2), 82.
Spath, L., 1936. The Upper Jurassic invertebrates faunas of Cape Leslie, Milne Lands, II, Upper Kimmeridgian and Portlandian. Medd. Grønland 99 (3), 180.
Spötl, C., Vennemann, T.W., 2003. Continuous-flow isotope ratio mass spectrometric analysis of carbonate minerals. Rapid Commun. Mass Spectrom. 17 (9), 1004–1006. https://doi.org/10.1002/rcm.1010.
Suan, G., Van De Schootbrugge, B., Adatte, T., Fiebig, J., Oschmann, W., 2015. Calibrating the magnitude of the Toarcian carbon cycle perturbation. Paleoceanography 30 (5), 495–509. https://doi.org/10.1002/2014PA002758.
Surlyk, F., 1977. Stratigraphy, tectonics and paleogeography of the Jurassic sediments of the areas north of Kong Oscars Fjord, East Greenland. Grønlands Geol. Undersøgelse Bull. 123, 56. https://doi.org/10.34194/bullggu.v123.6665.
Surlyk, F., 1978. Submarine fan sedimentation along fault scarps on tilted fault blocks (Jurassic-Cretaceous boundary, East Greenland). Grønlands Geol. Undersøgelse Bull. 128, 108. https://doi.org/10.34194/bullggu.v128.6670.
Surlyk, F., 1991. Sequence stratigraphy of the Jurassic-lowermost cretaceous of East Greenland. Am. Assoc. Pet. Geol. Bull. 75 (9), 1468–1488. https://doi.org/10.1306/0c9b296b-1710-11d7-8645000102c1865d.
Surlyk, F., 2003. The Jurassic of Denmark and Greenland: the Jurassic of East Greenland: a sedimentary record of thermal subsidence, onset and culmination of rifting. GEUS Bull. 1, 659–722. https://doi.org/10.34194/geusb.v1.4674.
Surlyk, F., Alsen, P., Bjerager, M., Dam, G., Engkilde, M., Hansen, C.F., Larsen, M., Noe-Nygaard, N., Piasecki, S., Therkelsen, J., 2021. Jurassic stratigraphy of East Greenland. GEUS Bull. 46, 116. https://doi.org/10.34194/geusb.v46.6521.
Sykes, R., Callomon, J., 1979. The *Amoeboceras* zonation of the Boreal upper Oxfordian. Palaeontology 22, 839–903.
Torsvik, T., Carlos, D., Mosar, J., Cocks, L., Malme, T.N., 2002. Global reconstructions and North Atlantic paleogeography 440 Ma to recent. In: Eide, E.A. (Ed.), BATLAS-Mid Norway Plate Reconstruction Atlas with Global and Atlantic Perspectives, pp. 18–39.
Ullmann, C.V., Korte, C., 2015. Diagenetic alteration in low-Mg calcite from macrofossils: a review. Geol. Quart. 59 (1), 3–20. https://doi.org/10.7306/gq. 1217. 10.7306/gq.1217.
Ullmann, C.V., Campbell, H.J., Frei, R., Hesselbo, S.P., von Strandmann, P.A.P., Korte, C., 2013a. Partial diagenetic overprint of late Jurassic belemnites from New Zealand: Implications for the preservation potential of δ7Li values in calcite fossils. Geochim. Cosmochim. Acta 120, 80–96. https://doi.org/10.1016/j.gca.2013.06.029.
Ullmann, C.V., Hesselbo, S.P., Korte, C., 2013b. Tectonic forcing of Early to Middle Jurassic seawater Sr/Ca. Geology 41 (12), 1211–1214. https://doi.org/10.1130/g34817.1.
Ullmann, C.V., Böhm, F., Rickaby, R.E., Wiechert, U., Korte, C., 2013c. The Giant Pacific Oyster (Crassostrea gigas) as a modern analog for fossil ostreoids: isotopic (Ca, O, C) and elemental (Mg/Ca, Sr/Ca, Mn/Ca) proxies. Geochem. Geophys. Geosyst. 14 (10), 4109–4120. https://doi.org/10.1002/ggge.20257.
Ullmann, C.V., Thibault, N., Ruhl, M., Hesselbo, S.P., Korte, C., 2014. Effect of a Jurassic oceanic anoxic event on belemnite ecology and evolution. Proc. Natl. Acad. Sci. 111 (28), 10073–10076. https://doi.org/10.1073/pnas.1320156111.
Ullmann, C.V., Frei, R., Korte, C., Hesselbo, S.P., 2015. Chemical and isotopic architecture of the belemnite rostrum. Geochim. Cosmochim. Acta 159, 231–243. https://doi.org/10.1016/j.gca.2015.03.034.
Ullmann, C.V., Boyle, R., Duarte, L., Hesselbo, S., Kasemann, S., Klein, T., Lenton, T., Piazza, V., Aberhan, M., 2020. Warm afterglow from the Toarcian Oceanic Anoxic Event drives the success of deep-adapted brachiopods. Sci. Rep. 10 (1), 1–11. https://doi.org/10.1038/s41598-020-63487-6.
van de Schootbrugge, B., Bailey, T.R., Rosenthal, Y., Katz, M.E., Wright, J.D., Miller, K. G., Feist- Burkhardt, S., Falkowski, P.G., 2005. Early Jurassic climate change and the radiation of organic- walled phytoplankton in the Tethys Ocean. Paleobiology 31, 73–97. https://doi.org/10.1666/0094-8373(2005)031<0073:EJCCAT>2.0.CO;2.
Veizer, J., 1983. Chemical diagenesis of carbonates: theory and application. Stable isotopes in sedimentary geology. Soc. Econ. Palaeontol. Mineral. Short Course 10, 3–100.
Veizer, J., Ala, D., Azmy, K., Bruckschen, P., Buhl, D., Bruhn, F., Carden, G.A., Diener, A., Ebneth, S., Godderis, Y., Jasper, T., 1999. 87Sr/86Sr, δ13C and δ18O evolution of Phanerozoic seawater. Chem. Geol. 161 (1–3), 59–88. https://doi.org/10.1016/S0009-2541(99)00081-9.
Vickers, M.L., Bajnai, D., Price, G.D., Linckens, J., Fiebig, J., 2019. Southern high-latitude warmth during the Jurassic–cretaceous: New evidence from clumped isotope thermometry. Geology 47 (8), 724–728. https://doi.org/10.1130/G46263.1.
Vickers, M.L., Fernandez, A., Hesselbo, S.P., Price, G.D., Bernasconi, S.M., Lode, S., Ullmann, C.V., Thibault, N., Hougaard, I.W., Korte, C., 2020. Unravelling Middle to late Jurassic palaeoceanographic and palaeoclimatic signals in the Hebrides Basin using belemnite clumped isotope thermometry. Earth Planet. Sci. Lett. 546, 116401 https://doi.org/10.1016/j.epsl.2020.116401.
Vickers, M.L., Bernasconi, S.M., Ullmann, C.V., Lode, S., Looser, N., Morales, L.G., Price, G.D., Wilby, P.R., Hougård, I.W., Hesselbo, S.P., Korte, C., 2021. Marine temperatures underestimated for past greenhouse climate. Sci. Rep. 11 (1), 1–9. https://doi.org/10.1038/s41598-021-98528-1.
Voigt, S., Wilmsen, M., Mortimore, R.N., Voigt, T., 2003. Cenomanian palaeotemperatures derived from the oxygen isotopic composition of brachiopods and belemnites: evaluation of cretaceous palaeotemperature proxies. Int. J. Earth Sci. 92, 285–299. https://doi.org/10.1007/s00531-003-0315-1.
Wierzbowski, A., 1989. Ammonites and stratigraphy of the Kimmeridgian at Wimanfjellet, Sassenfjorden, Spitsbergen. Acta Palaeontol. Pol. 34 (4), 355–378.
Wierzbowski, H., 2002. Detailed oxygen and carbon isotope stratigraphy of the Oxfordian in Central Poland. Int. J. Earth Sci. 91 (2), 304–314. https://doi.org/10.1007/s005310100217.
Wierzbowski, H., 2004. Carbon and oxygen isotope composition of Oxfordian–Early Kimmeridgian belemnite rostra: palaeoenvironmental implications for Late Jurassic seas. Palaeogeogr. Palaeoclimatol. Palaeoecol. 203 (1–2), 153–168. https://doi.org/10.1016/s0031-0182(03)00673-4.
Wierzbowski, H., Joachimski, M., 2007. Reconstructio of late Bajocian-Bathonian marine palaeoenvironments using carbon and oxygen isotope ratios of calcareous fossils from the Polish Jura Chain (Central Poland). Palaeogeogr. Palaeoclimatol. Palaeoecol. 254, 523–540. https://doi.org/10.1016/j.palaeo.2007.07.010.
Wierzbowski, H., Rogov, M., 2011. Reconstructing the palaeoenvironment of the Middle Russian Sea during the Middle–Late Jurassic transition using stable isotope ratios of cephalopod shells and variations in faunal assemblages. Palaeogeogr. Palaeoclimatol. Palaeoecol. 299 (1–2), 250–264. https://doi.org/10.1016/j.palaeo.2010.11.006.
Wierzbowski, H., Dembicz, K., Praszkier, T., 2009. Oxygen and carbon isotope composition of Callovian–Lower Oxfordian (Middle–Upper Jurassic) belemnite rostra from central Poland: a record of a Late Callovian global sea-level rise? Palaeogeogr. Palaeoclimatol. Palaeoecol. 283 (3–4), 182–194. https://doi.org/10.1016/j.palaeo.2009.09.020.
Wierzbowski, H., Rogov, M.A., Matyja, B.A., Kiselev, D., Ippolitov, A., 2013. Middle–Upper Jurassic (Upper Callovian–Lower Kimmeridgian) stable isotope and elemental records of the Russian Platform: indices of oceanographic and climatic changes. Glob. Planet. Chang. 107, 196–212. https://doi.org/10.1016/j.gloplacha.2013.05.011.
Wierzbowski, H., Bajnai, D., Wacker, U., Rogov, M.A., Fiebig, J., Tesakova, E.M., 2018. Clumped isotope record of salinity variations in the Subboreal Province at the Middle–Late Jurassic transition. Glob. Planet. Chang. 167, 172–189. https://doi.org/10.1016/j.gloplacha.2018.05.014.
Žák, K., Košťák, M., Man, O., Zakharov, V.A., Rogov, M.A., Pruner, P., Rohovec, J., Dzyuba, O.S., Mazuch, M., 2011. Comparison of carbonate C and O stable isotope records across the Jurassic/cretaceous boundary in the Tethyan and Boreal Realms. Palaeogeogr. Palaeoclimatol. Palaeoecol. 299 (1–2), 83–96. https://doi.org/10.1016/j.palaeo.2010.10.038.
Zhou, J., Poulsen, C., Pollard, D., White, T., 2008. Simulation of modern and middle cretaceous marine $\delta^{18}O$ with an ocean-atmosphere general circulation model. Paleoceanography 23, PA3223. https://doi.org/10.1029/2008PA001596.